buildings

MDPI

Article

Modelling of Cyclic Load Behaviour of Smart Composite Steel-Concrete Shear Wall Using Finite Element Analysis

Hadee Mohammed Najm [1,*], Amer M. Ibrahim [2,*], Mohanad Muayad Sabri [3], Amer Hassan [1], Samadhan Morkhade [4], Nuha S. Mashaan [5], Moutaz Mustafa A. Eldirderi [6] and Khaled Mohamed Khedher [7,8]

1 Department of Civil Engineering, Aligarh Muslim University, Aligarh 202002, India; ameralburay@gmail.com
2 Department of Civil Engineering, College of Engineering, University of Diyala, Diyala 32001, Iraq
3 Peter the Great St. Petersburg Polytechnic University, 195251 St. Petersburg, Russia; mohanad.m.sabri@gmail.com
4 Department of Civil Engineering, Vidya Pratishthan's Kamalnayan Bajaj Institute of Engineering & Technology (VPKBIET), Baramati, Pune 413133, India; samadhanmorhade@gmail.com
5 Faculty of Science and Engineering, School of Civil and Mechanical Engineering, Curtin University, Bentley, WA 6102, Australia; nuhas.mashaan1@curtin.edu.au
6 Department of Chemical Engineering, College of Engineering, King Khalid University, Abha 61421, Saudi Arabia; maldrdery@kku.edu.sa
7 Department of Civil Engineering, College of Engineering, King Khalid University, Abha 61421, Saudi Arabia; kkhedher@kku.edu.sa
8 Department of Civil Engineering, High Institute of Technological Studies, Mrezgua University Campus, Nabeul 8000, Tunisia
* Correspondence: gk4071@myamu.ac.in (H.M.N.); amereng76@yahoo.com (A.M.I.)

check for updates

Citation: Najm, H.M.; Ibrahim, A.M.; Sabri, M.M.; Hassan, A.; Morkhade, S.; Mashaan, N.S.; Eldirderi, M.M.A.; Khedher, K.M. Modelling of Cyclic Load Behaviour of Smart Composite Steel-Concrete Shear Wall Using Finite Element Analysis. *Buildings* **2022**, *12*, 850. https://doi.org/10.3390/buildings12060850

Academic Editor: Nerio Tullini

Received: 27 May 2022
Accepted: 13 June 2022
Published: 17 June 2022

Abstract: In recent years, steel-concrete composite shear walls have been widely used in enormous high-rise buildings. Due to their high strength and ductility, enhanced stiffness, stable cycle characteristics and large energy absorption, such walls can be adopted in auxiliary buildings, surrounding the reactor containment structure of nuclear power plants to resist lateral forces induced by heavy winds and severe earthquakes. The current study aims to investigate the seismic behaviour of composite shear walls and evaluate their performance in comparison with traditional reinforced concrete (RC) walls when subjected to cyclic loading. A three-dimensional finite element model is developed using ANSYS by emphasising constitutive material modelling and element type to represent the real physical behaviour of complex shear wall structures. The analysis escalates with parametric variation in reinforcement ratio, compressive strength of the concrete wall, layout of shear stud and yield stress of infill steel plate. The modelling details of structural components, contact conditions between steel and concrete, associated boundary conditions and constitutive relationships for the cyclic loading are explained. The findings of this study showed that an up to 3.5% increase in the reinforcement ratio enhanced the ductility and energy absorption with a ratio of 37% and 38%, respectively. Moreover, increasing the concrete strength up to 55 MPa enhanced the ductility and energy absorption with ratios of 51% and 38%, respectively. Thus, this improves the contribution of concrete strength, while increasing the yield stress of steel plate (to 380 MPa) enhanced the ductility (by a ratio of 66%) compared with the reference model. The present numerical research shows that the compressive strength of the concrete wall, reinforcement ratio, layout of shear stud and yield stress of infill steel plate significantly affect ductility and energy absorption. Moreover, this offers a possibility for improving the shear wall's capacity, which is more important.

Keywords: composite steel plate shear wall; hysteresis curves; ductility; energy absorption; ANSYS

1. Introduction

During earthquakes, buildings located in seismic zones are at risk of extensive damage [1]. To dissipate the rate of hysteretic seismic energy without a significant loss of lateral strength and stiffness, structural elements must be endowed with ductility [2–4]. Since reinforced concrete walls have a high structural performance, they can effectively limit the building's lateral displacements during a seismic event and minimise the level of damage [5]. Various structural and architectural parameters (such as the height-to-length ratio, the existence of openings, cross-sectional arrangements and materials) highly influence the load-bearing capacity of such elements simultaneously and could also modify their nonlinear behaviour [6,7]. Moreover, in many cases, due to architectural requirements, walls may have complex shapes and require high steel ratios for increased bearing capacity, which increases wall construction time. In recent decades, extensive research has been done to develop an effective and economical solution to improve the structural performance and technological issues of reinforced concrete structural walls [8,9].

The components of composite steel plate shear walls (CSPSW) consist of web plates, infill steel plates, concrete and shear studs. A composite steel plate shear wall proves to be excellent over reinforced concrete walls in terms of ultimate strength, stiffness, ductility and energy dissipation [10].

Previous researchers have shown a lot of interest in the use of composite steel plate shear walls in buildings [11–13]. The appropriate provisions for composite shear walls, such as various seismic composite shear walls including ASCE 7-10 and AISC 341-10 [14,15], have been prepared by allowing the use of CSPSW systems in earthquake zones. The researchers have conducted numerous experimental tests to study the behaviour of composite shear walls in the absence of boundary walls. Nie et al. [16], Mydin [17], Wright [18] and Wang [19] depict a situation in which composite shear walls not only have a very high ultimate strength but also excellent ductile behaviour. The local buckling of the web and fracture failure of corners of the wall are the observed failure modes. Zhang et al. [20] and Zhang et al. [21] showed that more channels lead to reductions in the ultimate strength and stiffness of the wall but a substantial observed improvement in ductile and energy dissipation behaviour. Finally, calculating the ultimate strength and initial stiffness has been proposed, but all the necessary variables are not included in the proposed equation, which leads to conservative results and this therefore creates a strong demand to perform an exhaustive numerical analysis of composite shear wall [22,23].

Many researchers have suggested equation-based FE analysis for composite shear walls. Nguyen et al. [24], Epackachi et al. [25] and Rafiei et al. [26] established the finite element models and checked their accuracy. Wei et al. [27] show the axial compression performance of composite shear walls. The higher axial compression ratio of the wall is beneficial for restraining the internal concrete and improving the compressive strength of the concrete. Thus, the energy dissipation capacity of the composite shear wall is enhanced [28,29] Increasing the thickness of the steel plate can increase the stiffness and ultimate bearing capacity of the wall, as the hysteretic curve of the wall is plumper [30–33]. Epackachi et al. [34] simulated shear walls with different aspect ratios. When the aspect ratio was between 0.6 and 3.0, the coupling effect of the moment and shear force was obvious. The specifications [15,35–37] define the formula for the shear capacity of composite shear walls. The formulas for the shear and flexural capacity were given, but the formula for estimating the flexural-shear coupling was not provided [38].

Khatir et al. [39] proposed two-stage approaches for studying damage detection, localization and quantification in functionally graded material (FGM) plate structures. Metal and ceramic FGM plates were considered using three different composite materials. The results show that the improved indicator can predict the damaged elements with high precision. Saadatmorad et al. [40] proposed a method called the wavelet transform-based convolutional neural network (WT-CNN) technique for damage detection of rectangular laminated composite plates (RLCPs). The results show that the proposed method can predict and detect the location of damage in RLCPs with high accuracy and eliminate problems of trial and error simulations for future input signals of damaged RLCPs. Khatir et al. [41] studied an improved frequency response function (FRF) indicator for damage identification in complex structures. To verify the effectiveness of the improved damage indicator, different structures were used. The results showed that all optimization techniques can accurately predict the exact level of damage. However, an artificial gorilla troops optimizer (GTO) is the most efficient in terms of convergence. To study the effectiveness of this indicator in the case of noisy data, different levels of noise are considered in the damage assessment exercises. To the authors' knowledge, the seismic performances of such wall configurations have not been extensively studied, and the research on this type of topic is quite scarce. This study investigates the seismic performance of structural steel-concrete composite shear walls numerically. Four different factors that affect shear wall behaviour were studied in this paper. To assure the effect of all possible factors between the boundary steel profiles and reinforced concrete web panels of the walls, the ratio of reinforcement, compressive strength of the concrete wall, yield stress of infill steel plate and layout of a shear stud was considered. Considering the numerical issues that could generally appear in the modelling phase of the steel plate and concrete walls due to the complexities of the steel and concrete behaviours and their interaction. The seismic behaviour, stiffness, ductility and energy absorption are discussed and compared between the tested specimens and numerical models.

2. Experimental Work

2.1. Sample Design

The experimental work conducted on CSPSW was carried out by Rahai and Hatami [42] to study the behaviour of composite shear walls made of concrete and steel. The details of the experimental work of CSPSW are shown in Figure 1.

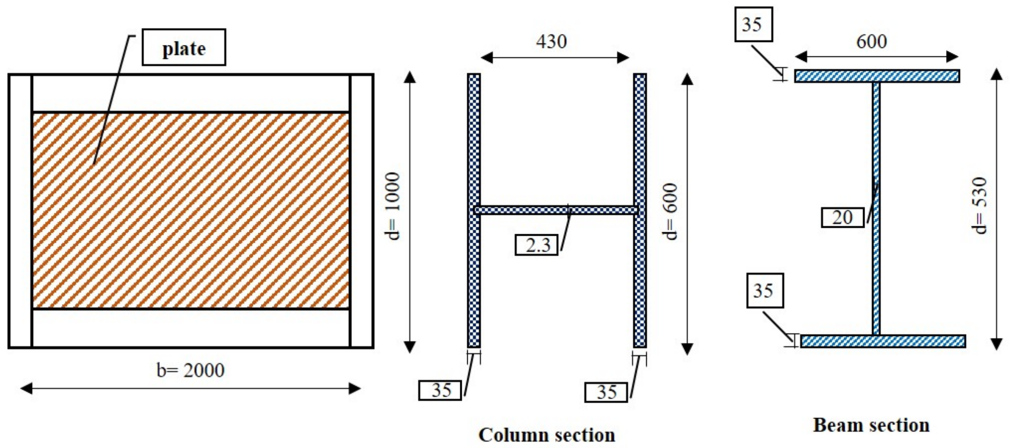

Figure 1. Experimental Specimen Dimensions.

The length of frame span that is, the centre distance to the centre of both sides' column, is 2000 mm, and the height is also frame 1000 mm, which is the centre distance to the centre of the top and bottom beams. Columns and beam sections were also double IPE2000 that were reinforced with two plates (150 × 12 mm) on the flanges. Steel plate was inscribed inside the boundary beams and columns. It is 1776 mm wide, and the thickness of these plates is also considered 3 mm. The thickness of the concrete cover is 50 mm.

There is a 30 mm gap between the concrete cover and the boundary elements, 1716 × 1716 mm in length and width. In order to connect the concrete cover of 50 mm thickness to a steel plate using 7 mm diameter and 100 mm length bolts, and also to reinforce the concrete cover of thickness 50 mm, 6.5 mm diameter bars with a centre distance to the centre 65 mm were used [31].

Table 1 shows the characteristics and strength of steel that is used in all models: St37 with a yield stress of 240 MPa and ultimate stress of 370 MPa. The behaviour of the steel is considered a bilinear elastic-plastic curve for modelling. The compressive strength of concrete in a 28-day cylindrical core sample is about 45 MPa, and the tensile strength is equivalent to 3 MPa.

Table 1. Details of the experimental specimens and mechanical properties.

Group No.	Group Name	SW	Gap	Thickness of Steel	Thickness of Concrete	Distance between Shear Stud	Ratio of Reinforcement	Compressive Strength	Yield Strength	The Layout of Shear Stud (H × V)
1	Ratio of reinforcement	SW-RR1% (R)	40	3	50	200	1%	45	240	3 × 8
		SW-RR1.5%	40	3	50	200	1.5%	45	240	3 × 8
		SW-RR2.5%	40	3	50	200	2.5%	45	240	3 × 8
		SW-RR3.5%	40	3	50	200	3.5%	45	240	3 × 8
2	Compressive strength of concrete wall	SW-CS45MPa (R)	40	3	50	200	1%	45	240	3 × 8
		SW-CS25MPa	40	3	50	200	1%	25	240	3 × 8
		SW-CS28MPa	40	3	50	200	1%	28	240	3 × 8
		SW-CS50MPa	40	3	50	200	1%	50	240	3 × 8
		SW-CS55MPa	40	3	50	200	1%	55	240	3 × 8
3	Yield stress of infill steel plate	SW-R	40	3	50	200	1%	45	240	3 × 8
		SW-YS150MPa	40	3	50	200	1%	45	150	3 × 8
		SW-YS200MPa	40	3	50	200	1%	45	200	3 × 8
		SW-YS350MPa	40	3	50	200	1%	45	350	3 × 8
		SW-YS380MPa	40	3	50	200	1%	45	380	3 × 8
4	Layout of shear stud	SW-R	40	3	50	200	1%	45	240	3 × 8
		SW-L8*3	40	3	50	200	1%	45	240	3 × 8
		SW-L6*4	40	3	50	200	1%	45	240	6 × 4
		SW-L4*6	40	3	50	200	1%	45	240	4 × 6
		SW-L2*12	40	3	50	200	1%	45	240	2 × 12

2.2. Loading Programme and Test Setup

Horizontal loading was controlled by force [42]. In the force loading phase, the horizontal forces were 600 kN, and loading was cyclically loaded with 1/60 Hz frequency. The experimental load characteristics are shown in Table 2. The loading history is illustrated in Figure 2.

Table 2. Cyclic loading time history.

Time (Second) Start	End	Max. Load (KN)	Loading Shape	Frequencies (Hz)
0.0	71	0.0	Cyclic	0
72	180	300	Cyclic	1/60
181	360	500	Cyclic	1/60
361	540	600	Cyclic	1/60

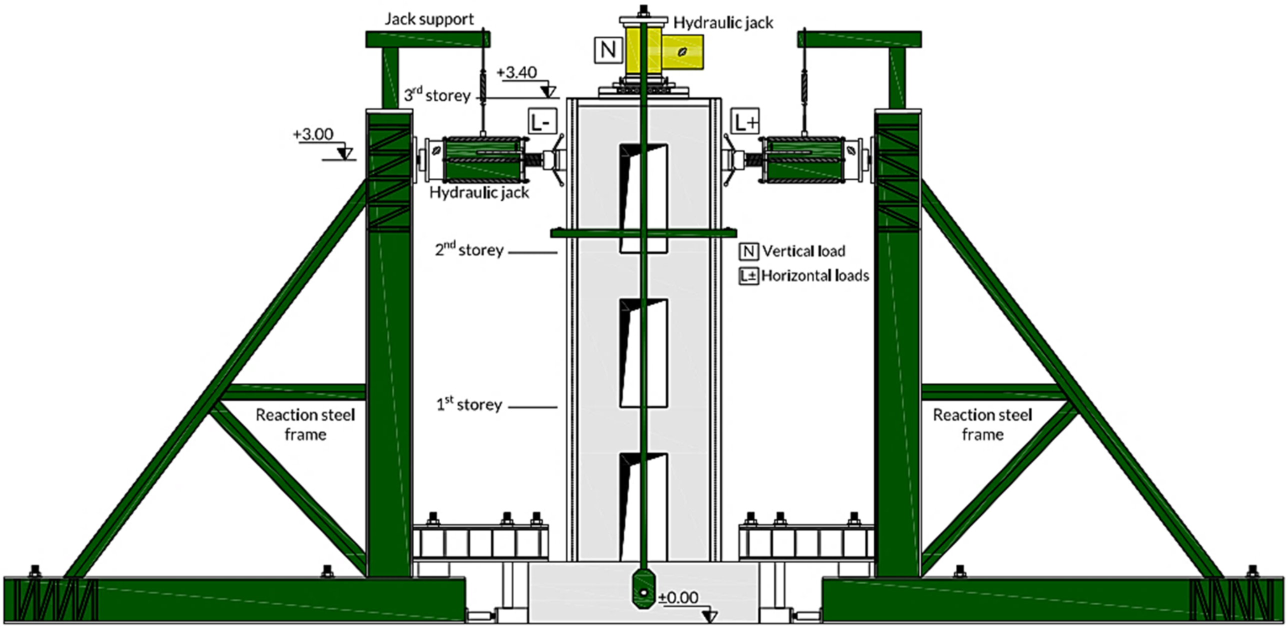

Figure 2. Cyclic loading arrangement.

3. Finite Element Model (FEM)

3.1. Model Overview

3.1.1. Part and Element of the FE Model

The numerical study is performed by finite element analysis using ANSYS. The finite element model consists of five parts, the infilled steel plate, shear studs, outer steel frame, reinforced concrete wall and reinforcement. The outer steel frame consists of a web and flange plate.

A total of 181 four-noded shell elements from the ANSYS element library were used to model the outer steel frame, infilled plate, web and flange plate. The element has six degrees of freedom at each node. The change in stress in the thickness direction cannot be ignored in shear stud and concrete walls because the sizes in the three directions have little difference. Therefore, the element choice to represent the shear stud and reinforcement was a link 180. The element used to represent the concrete wall was 3D solid65. In the test, the shear studs were welded on the web plate. Thus, the shear studs are tied to the steel plate in the FE model. In the test, the reinforcement and the steel studs were fixed in the concrete.

3.1.2. Contact of FE Mode

A friction contact model has been used between the steel plate and concrete. The tangential friction coefficient is 0.6 [43], as shown in Figure 3a. The interface surface between infill steel plate and concrete wall is represented by targe170 and contact 174. Finally, the load slip action is represented by comb 39, as shown in Figure 4. The assembled FE model is shown in Figure 3e.

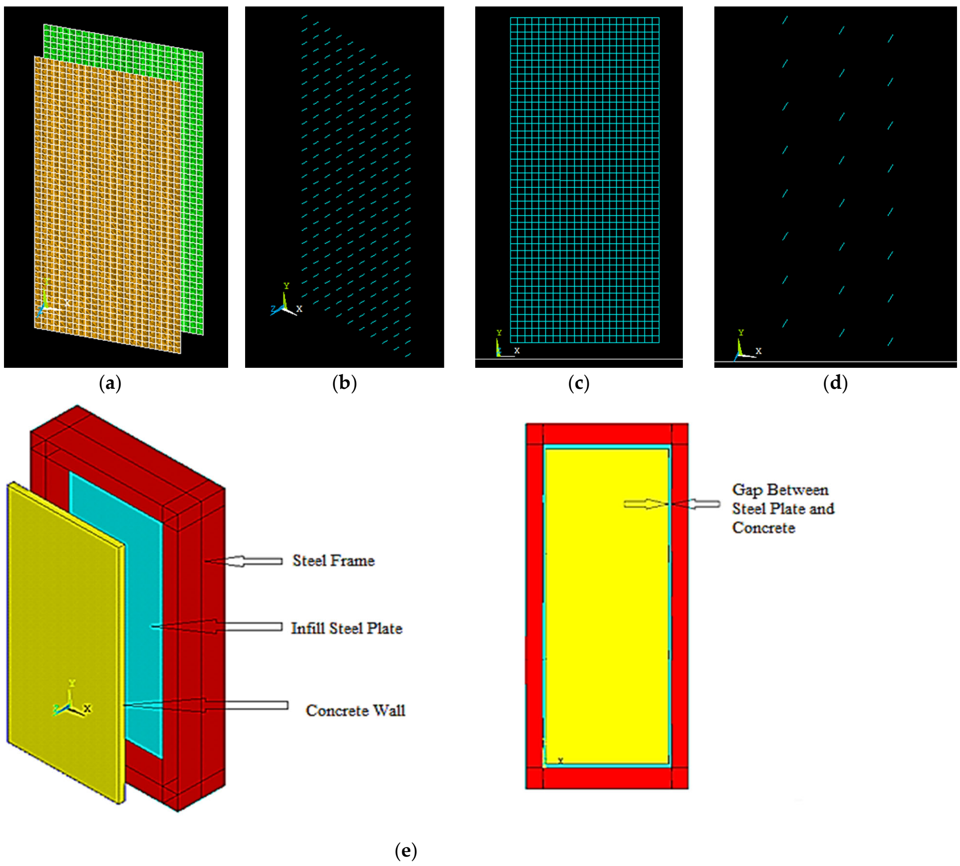

Figure 3. Contact between different elements: (**a**) interface surface; (**b**) load slip; (**c**) reinforcement; (**d**) shear stud; (**e**) assembled FEM.

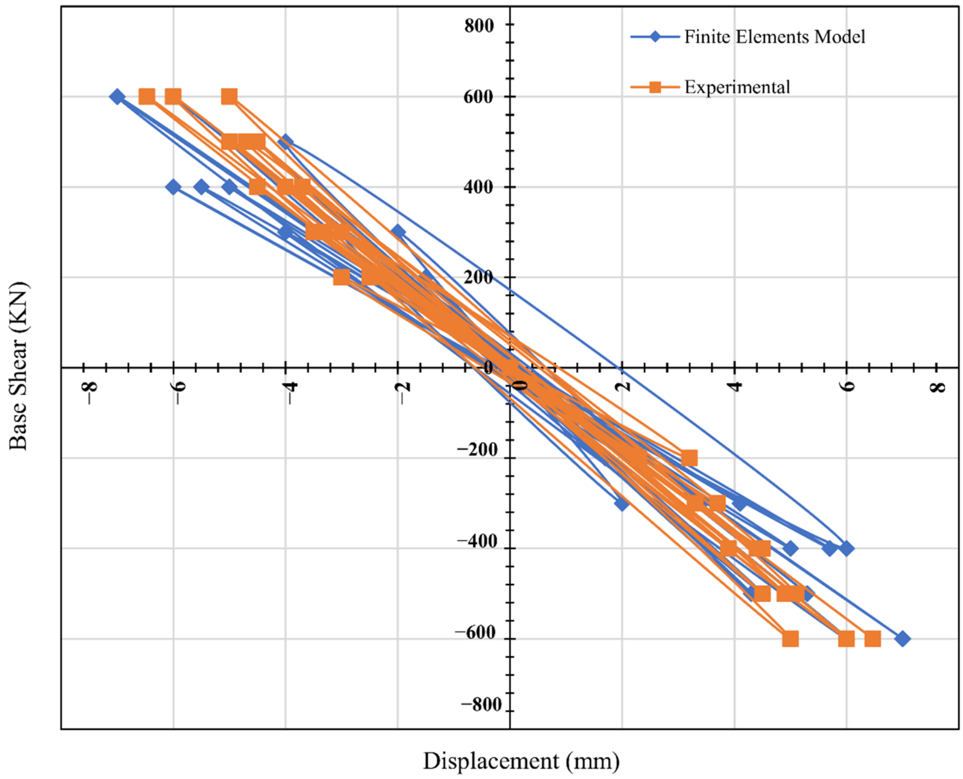

Figure 4. Comparison of deformation-load in the numerical and experimental model for CSPSW.

3.1.3. Boundary Conditions

The bottom frame is a fixed end constraint, and the boundary condition of the top beam is a sliding constraint. Therefore, six degrees of freedom are constrained at the bottom steel frame (i.e., U1 = U2 = U3 = UR1 = UR2 = UR3 = 0), and four degrees of freedom are constrained at the top steel frame (i.e., U3 = UR1 = UR2 = UR3 = 0).

3.1.4. Steel Constitutive Model

Steel plate is a major element in the composite shear wall. Preferably, for this plate steel with a low yield point is chosen. For example, an St37 steel plate is preferred for high strength steel plate because an St37 steel plate, due to its low yield point, is preferred to encourage the yielding of steel plates.

3.1.5. Concrete Constitutive Model

The reinforced concrete cover on one or both sides of a steel plate carry some of the story shear by improving the diagonal compression field and increasing strength and stiffness. Of course, the major role of the reinforced concrete cover is to prevent the out-of-plan buckling of the steel plate prior to yielding. In some cases, shear studs are not only subjected to shear but also to a considerable tension due to local buckling of the steel plate. For cast-in-place concrete, welded shear studs are usually utilised; for pre-cast concrete walls, bolts can be used.

3.2. Validation of Finite Element Model

Before performing an actual parametric study, the validation of the FE model was performed. The results of hysteretic curves obtained from FE analysis and test results comparison are shown in Figure 4. It is observed that the FE results closely match with test results. Therefore, it is concluded that the FE model is able to simulate the hysteretic curves of the composite steel plate shear wall in a significant approach.

In the test loading process, the steel plate experienced severe buckling at different positions with increasing horizontal displacement as shown in Figure 5. The FE model could simulate the local buckling phenomenon, as shown in Figure 6.

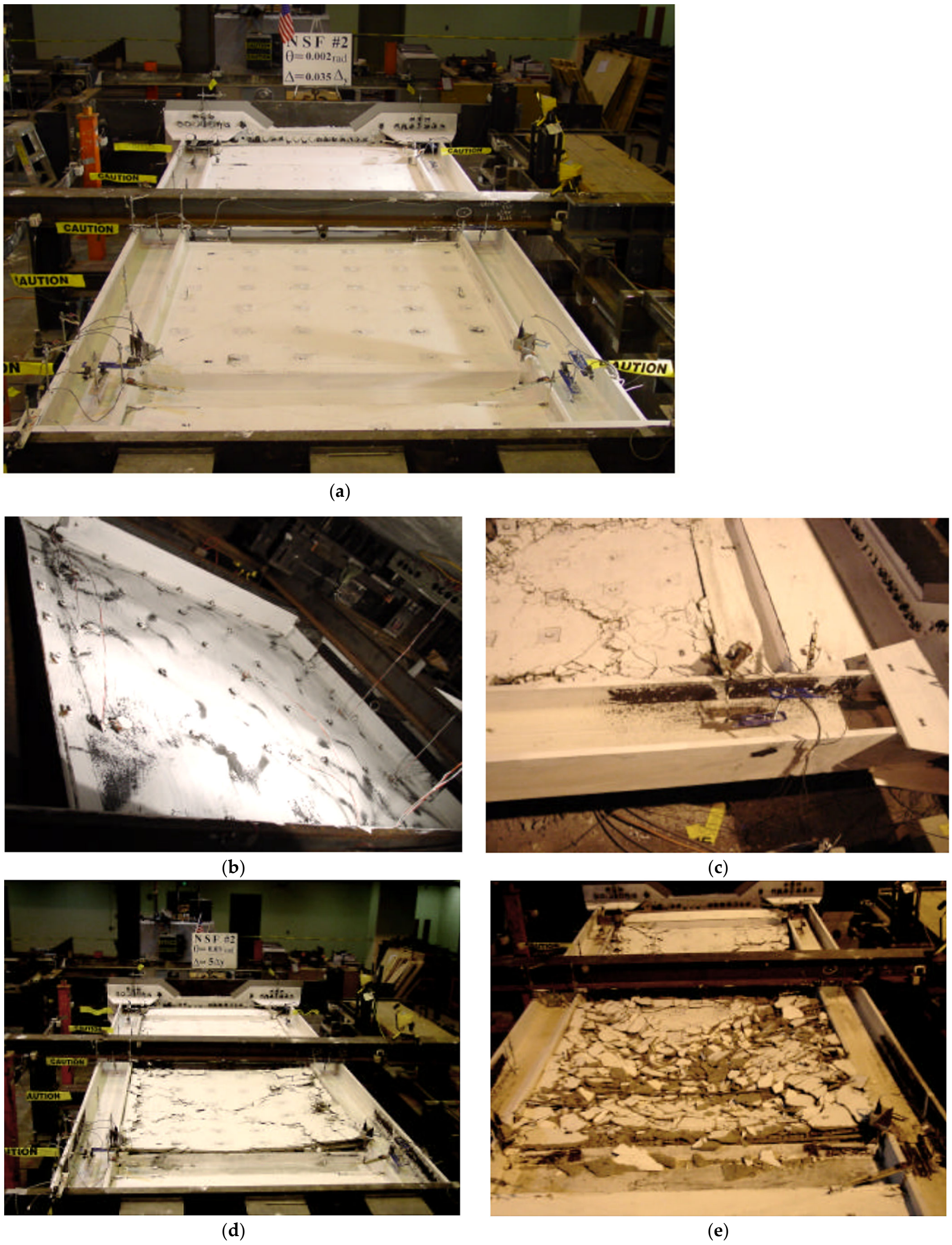

Figure 5. Local buckling, out-of-plane and crack formation for experimental specimen. (**a**) A View of Test Specimen (**b**) steel plate buckling; (**c**) plastic hinge at the base of column; (**d**) concrete crack at mid of the test; (**e**) concrete crack at end of the test.

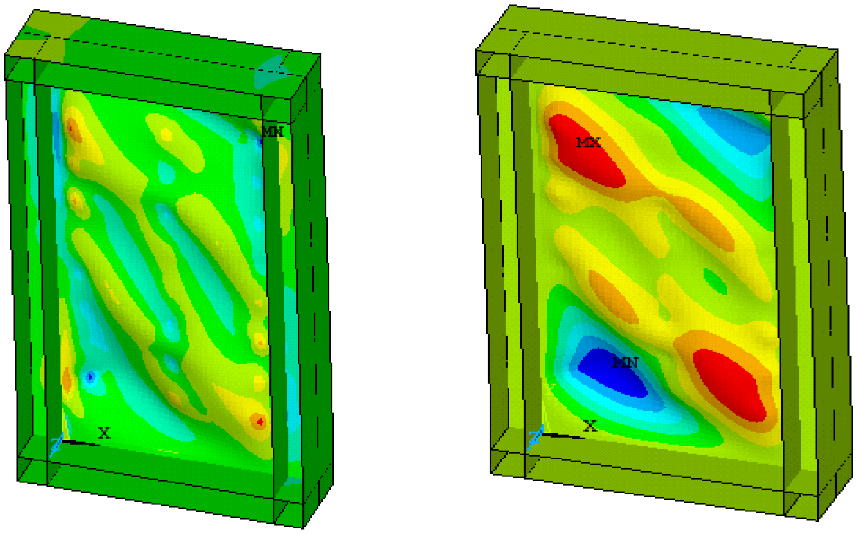

Figure 6. Local buckling, out-of-plane deflection for numerical specimen.

The results obtained during the last cyclic loading from the experimental and the ANSYS output are presented in Figures 5–7, which show the comparison of out-of-plane deflection and crack formation in the composite shear wall in different experimental and numerical specimens. The lateral displacement was found to be 6.47 mm and 7 mm in the case of numerical and experimental tests, respectively.

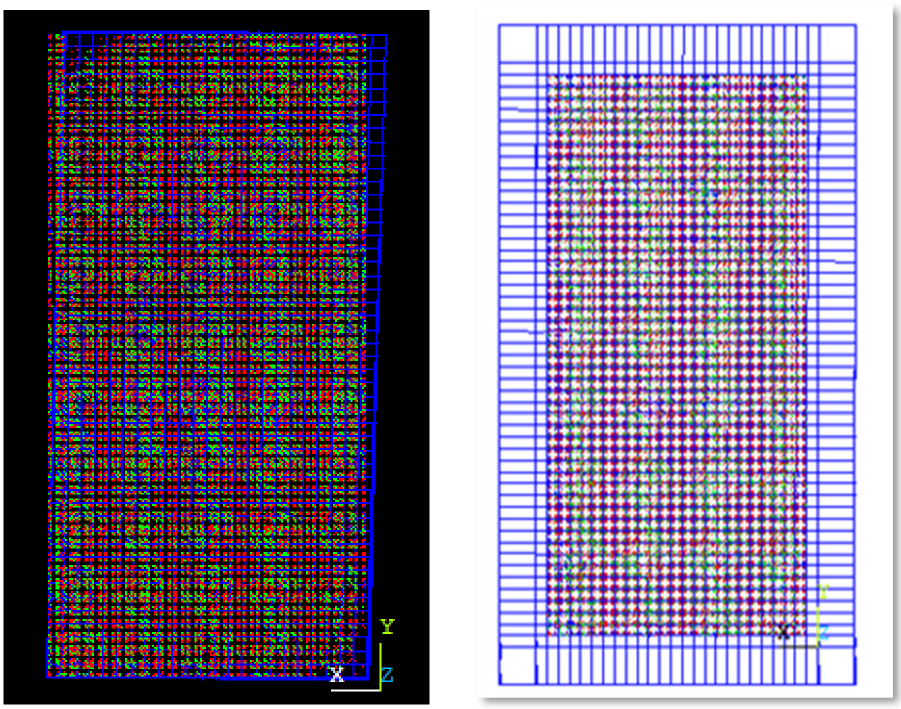

Figure 7. Concrete crack formation for numerical specimen.

4. Parametric Analysis

For optimisation of shear wall parameters in tall structures, the parametric study has been performed by varying the section size, and design guidelines have been suggested [42]. The effects of different variables have been vitally studied on stiffness, ductility, and energy dissipation of the composite shear wall. To study the hysteric behaviour of the model in parametric analysis, the cyclic load is applied to the wall. The boundary conditions in the model are consistent with the test.

The variables consist of the gap between the concrete wall and steel frame, the thickness of the infill steel plate, the concrete wall, the distance between the shear stud, the ratio of reinforcement, concrete strength, steel yield strength and the layout of a shear stud. The standard model parameters are chosen as follows: the gap between the concrete wall and steel frame is about 40 mm, the concrete wall thickness is about 50 mm, the steel ratio is 1%, infill steel plate thickness is about 3 mm, the distance between shear stud is 200 mm, the axial compressive strength of the concrete is 45 MPa and the yield strength of the infill steel plate is 240 MPa; the layout of the shear stud is (H*V) (3×8).

In the parametric analysis, the ratio of reinforcement ranges (1–1.5–2.5–3.5%), the axial compressive strength of the concrete ranges (25–28–45–50–55 MPa), the yield strength of the infill steel plate ranges (150–200–240–300–350–380 MPa) and the layout of shear stud ranges (3×8, 8×3, 6×4, 4×6, 2×12, 12×2) ($H \times V$).

4.1. Influence Rules of the Parameters

The influence rules of key design parameters are studied by including material displacement, stiffness, ductility and energy dissipation. The structural behaviour of the composite steel plate shear wall, when subjected to cyclic load, is characterised by four different stages with an increasing load applied; these stages are:

- The initial elastic stiffness phase
- The shear yielding stiffness phase
- The post yielding stiffness phase
- The pre-failure stiffness phase

The smart CSPSW, at first loading, shows a linear elastic response where the steel frame and infill steel plate, beams and columns, undergo inelastic deformations.

After that, the interaction between the infill steel plate and the reinforced concrete panel in the compression field is particularly efficient. While the lateraling loading is more raised, the infill steel plate responsible is immaterially and geometrically nonlinear. Moreover, the lateral shear stiffness of the wall drops substantially owing to the shear yield of the infill steel plate.

During the third phase, with the excess of lateraling unloading, the pure shear yield transpires pending the fully shear yield appearing in the infill steel plate, and the lateral stiffness is reduced gradually at this phase.

While the lateral load surpasses the shear yield capacity of the infill steel plate, the material and geometric nonlinearity responsible for steel frame and boundary elements is massive. At this phase, the frame supplies the utmost lateral stiffness.

The test results appear to show that increasing the model thickness (infill steel plate and concrete wall) worked to increase the structural strength capacity and the model's ability to absorb and dissipate energy which led to delaying the model's failure; at the same time, it prevented a rapid drop in the load-carrying capacity.

Additionally, increasing the distance and layout of the shear stud (certified number of shear studs) increased the structural strength capacity and enhanced the ability of the model to absorb energy and the model's ductility.

What is more, when the properties of smart CSPSW are increased the structural strength capacity and model's ability to absorb and dissipate energy are enhanced.

4.1.1. The First Group Models (Influence of Reinforcement Ratio)

1. Lateral displacement

Figure 8 shows that the models SW-RR1.5%, SW-RR2.5% and SW-RR3.5% go through the same phases as the reference model SW-RR1% (R) when loaded gradually and each phase has been discussed below. Furthermore, the effect of the reinforcement ratio on the out-of-plane displacement of group 1 is shown in Figure 9.

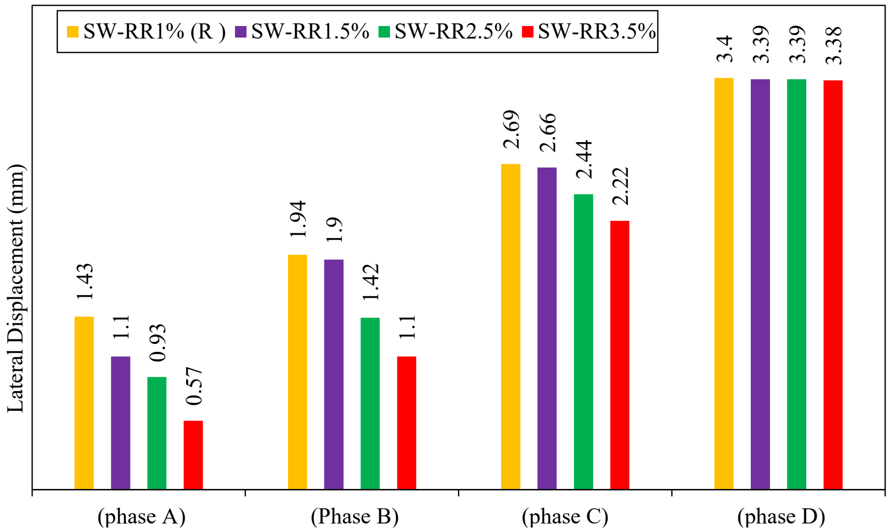

Figure 8. Lateral displacement of group 1.

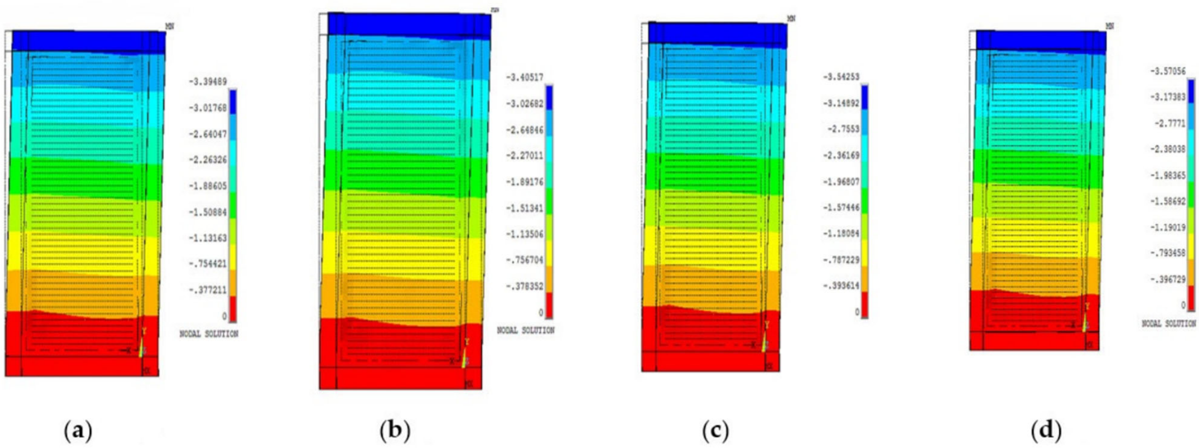

Figure 9. Effect of reinforcement ratio (RR) on the lateral displacement, (**a**) RR = 1%, (**b**) RR = 1.5%, (**c**) RR = 2.5%, (**d**) RR = 3.5%.

- Phase A:

From this phase, it can be noted that the change in the material properties of the concrete wall represented by the ratio of reinforcement (ρ) affected the elastic phase significantly for the model; therefore, the lateral displacement value of the models (SW-RR1.5%, SW-RR2.5%, SW-RR3.5%) at the same load decreased by 23%, 34% and 60 % as compared to the reference model SW-R. This enhancement in the wall capacity of the models may be due to the material properties of the concrete wall.

- Phase B:

This phase is characterised by high applied loads with a slight change in the lateral displacement, where the models (SW-RR1.5%, SW-RR2.5%, SW-RR3.5%) have a lower lateral displacement by 2, 26 and 43% as compared to the reference model SW-R. This is due to the material properties of the concrete wall represented by the ratio of reinforcement (ρ) being directly proportional to the load-carrying capacity of the model.

- Phase C:

When there is an increase in lateral load, the shear yield propagates until the full shear yield occurs in the infill steel plate. In this phase, when changing the ratio of reinforcement for SW-RR1.5%, SW-RR2.5% and SW-RR3.5%, the lateral displacement was enhanced (by 1, 9, 17%) as compared to the reference model SW-R.

- Phase D:

This phase begins at the ultimate load, where a high increase in the lateral displacement occurs, leading to a large buckling in the steel plate and cracking in a concrete wall. The change in material properties of the concrete wall is represented by the ratio of reinforcement (ρ) (for SW-RR1.5%, SW-RR2.5%, SW-RR3.5%); under the same cycle of loading, the lateral displacement decreases by 0.29, 0.29 and 0.59%.

2. Stiffness

The stiffness values of the fifth group model are shown in Figure 10. From the results, it is stated that increasing the ratio of reinforcement of the models does not influence stiffness because of the convergence of lateral displacement values. Therefore, the stiffness of the modelled SW-RR1.5%, SW-RR2.5% and SW-RR3.5% is substantial being about 0.24, 0.24, and 0.58 % as compared to the reference model SW-R.

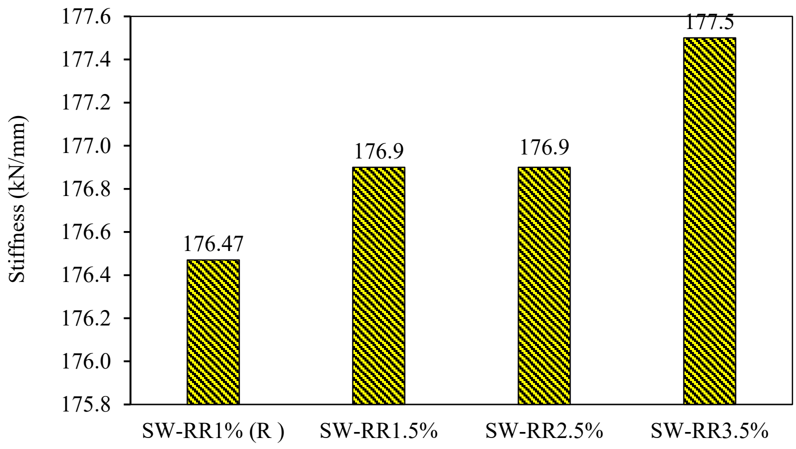

Figure 10. Stiffness of Group 1.

3. Ductility

The change in the material properties of the concrete walls is represented by the ratio of reinforcement (ρ) of the models affected by their ductility. Figure 11 gives the ductility values of the fifth group models. From this figure, the model (SW-RR1.5%, SW-RR2.5%, SW-RR3.5%) has greater ductility (by 1, 36, 75%) as compared with the reference model SW-R. From the results, it appears that there is a proportional relationship between the ductility and material properties of concrete walls. Therefore, increasing the ratio of reinforcement causes an increase in the ductility and ultimately gives a gradual drop in the load-carrying capacity until the fracture load is reached.

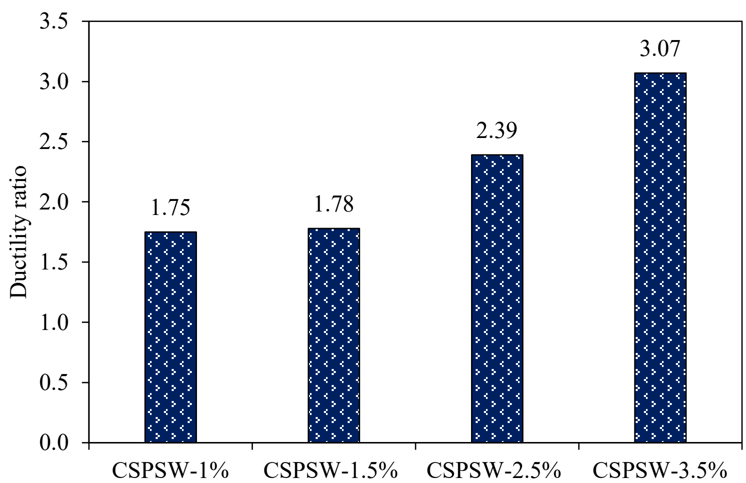

Figure 11. Ductility ratio of group 1.

4. Energy Absorption

The energy absorption of each model through the final phase is shown in Figure 12. For (SW-RR1.5%, SW-RR2.5% and SW-RR3.5%) in phase C, when there is an increase in the ratio of reinforcement, the energy absorption increases (by 14, 17 and 19%, respectively) as compared with the reference model SW-R. Through phase D, it can be noticed that an increased ratio of reinforcement increased the energy absorption (by 10, 27 and 38%) for SW-RR1.5%, SW-RR2.5% and SW-RR3.5% as compared with reference model SW-R. The models with a high ratio of reinforcement (SW-RR3.5%) have good energy absorption, and this was due to the high area under the curve of load deflection and it refers to the increased resistance of the model to the deformation.

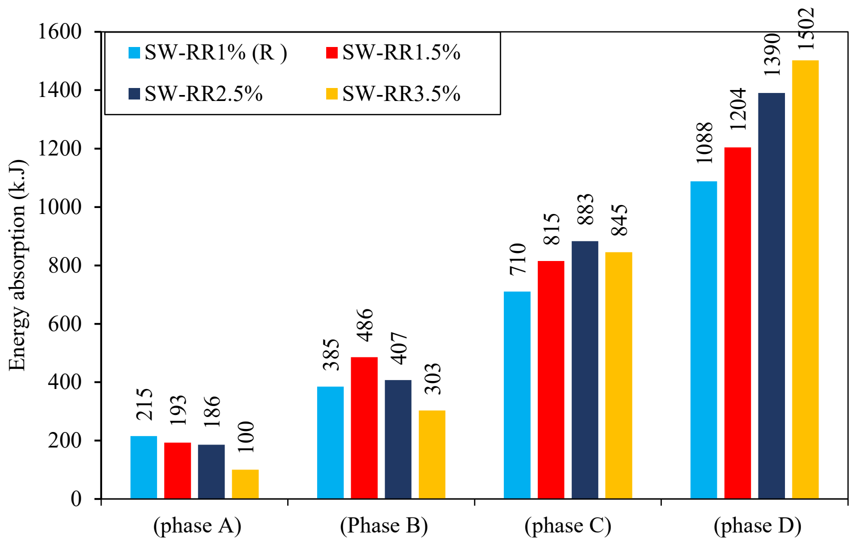

Figure 12. Energy absorption of group 1.

From the calculation of stiffness, ductility and energy absorption, it can be seen that the ratio of reinforcement has an obvious effect on the behaviour of smart CSPSW because the increasing ratio of reinforcement leads to a gradual drop in the load-carrying capacity until the fracture load is reached.

From the results of the phases above, it can be noticed that the ratio of reinforcement wall should be limited to some specific value (max. 3.5%) because the behaviour of smart CSPSW remains the same beyond that ratio. Thus, the ideal range for using the thickness of the concrete wall is between (1–3.5%).

4.1.2. The Second Group Models (Influence of Concrete Wall Compressive Strength)

1. Lateral Displacement

Figure 13 shows the behaviour of the second model, SW-CS25MPa, SW-CS28MPA, SW-CS50MPa and SW-CS55MPa, in terms of lateral displacement. Additionally, the out-of-plane displacement of each model of group 2 is shown in Figure 14. The loading and displacement phases of group 2 are presented below.

- Phase A:

From this phase for SW-CS25MPa and SW-CS28MPa, it is noted that the decreasing of the material properties of concrete walls represented by compressive strength increased the values of the lateral displacement significantly (by 34, 34%) and led to a decrease in the elastic phase. For the models SW-CS50MPa and SW-CS55MPa, it is noted that the increase in the material properties of concrete wall decreased the values of the lateral displacement significantly (by 30, 58%) and led to an increase in the elastic phase.

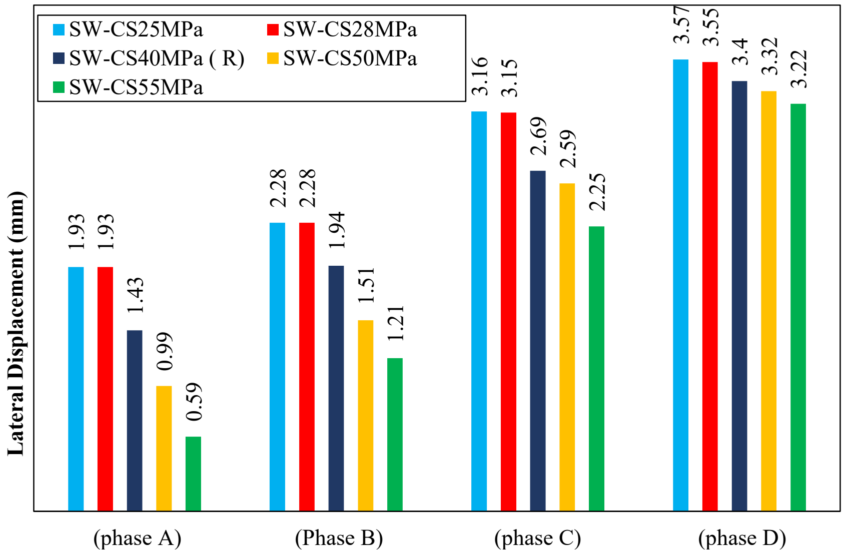

Figure 13. Lateral displacement of group 2.

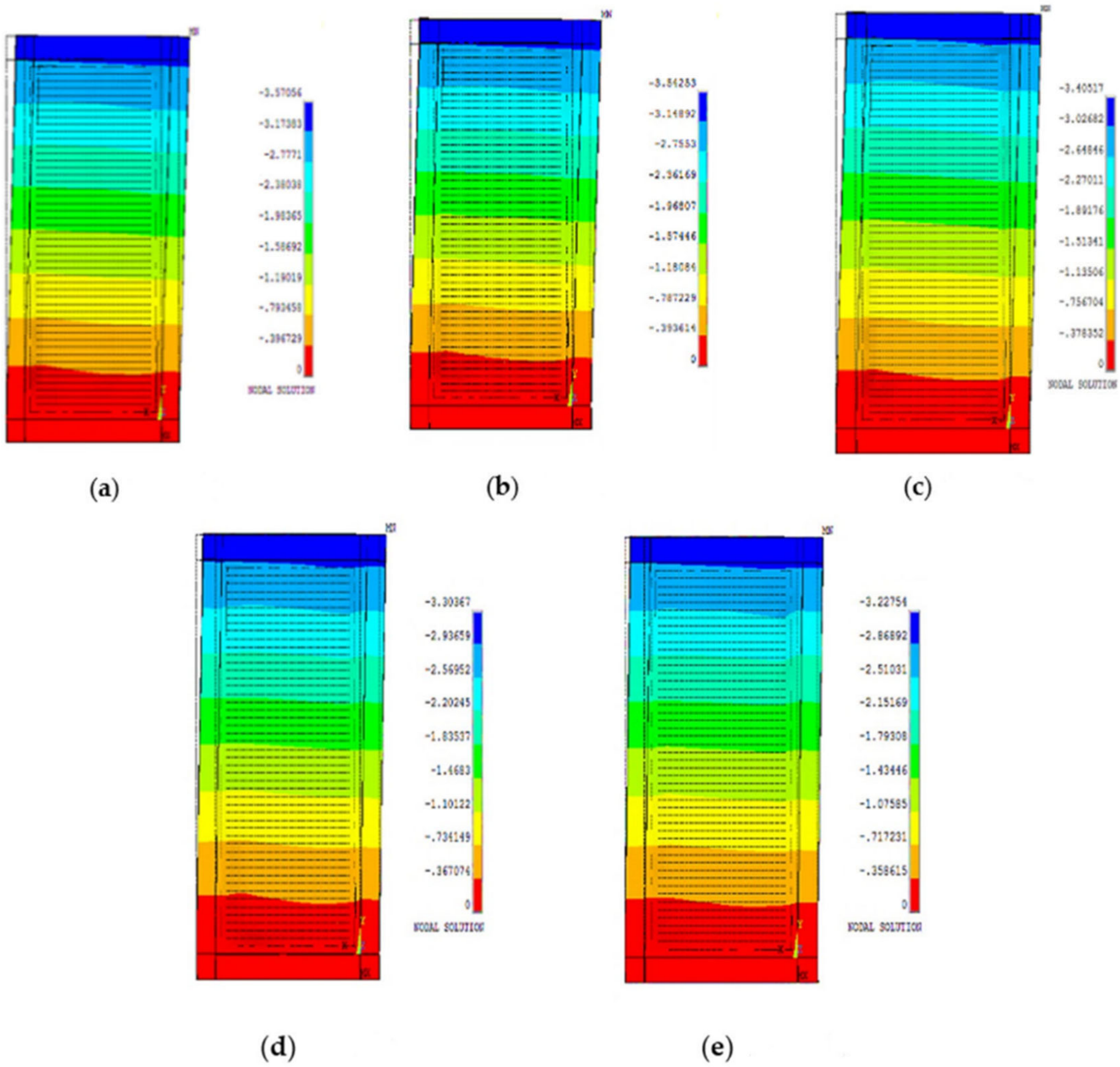

Figure 14. Effect of compressive strength (CS) of concrete on the lateral displacement, (**a**) CS = 25 MPa, (**b**) CS= 28 MPa, (**c**) CS = 45 MPa, (**d**) CS = 50 MPa, (**e**) CS = 55 MPa.

- Phase B:

For models SW-CS25MPa and SW-CS28MPa, it is noted that decreased material properties of concrete walls represented by compressive strength (F'_c) are directly proportional to the value of lateral displacement, which increases (by 17, 17%) compared to the reference model SW-CS28MPa(R). While for models SW-CS50MPa and SW-CS55MPa, it is noted that increased material properties of concrete walls are represented by compressive strength, (F'_c) is directly proportional to the value of lateral displacement, which decreases by 22 and 37% in comparison with the reference model SW-CS28MPA(R).

- Phase C:

In this phase, when decreasing the compressive strength (from 45 to 25 MPa) for SW-CS25MPa and SW-CS28MPa, the lateral displacement is larger (by 15, 14.6%) as compared with the reference model SW-CS45MPa (R), where this large displacement leads to a sudden drop in the model. When there is an increase in the compressive strength (from 45 to 55 MPa) for SW-CS50MPa and SW-CS55MPa, the lateral displacement was lower (by 4, 20%) as compared with the reference model SW-CS45MPa (R)

- Phase D:

In this phase, the models SW-CS25MPA, SW-CS28MPA, SW-CS50MPA and SW-CS55MPA have very similar behaviour with very close values of lateral displacement. It is noted that the decrease or increase in compressive strength did not have any large effect on phase D for these models. Continuing the model loading worked on the development of pure shear yield in the steel plate. From this, it appears that increasing the compressive strength of the concrete wall delays the failure of smart CSPSW.

2. Stiffness

Figure 15 gives the stiffness values for the sixth group of models, which shows that the stiffness is directly proportional to the increased compressive strength of the concrete wall. The model SW-CS55MPA, with compressive strength equal to 55 MPa, has a high stiffness of up to 186.34 kN/mm because of the small lateral displacement at ultimate load, while the model SW-CS25MPA with compressive strength equal to 25 MPa has a low stiffness equal to 168.07 kN/mm because of the elevated lateral displacement at the ultimate load.

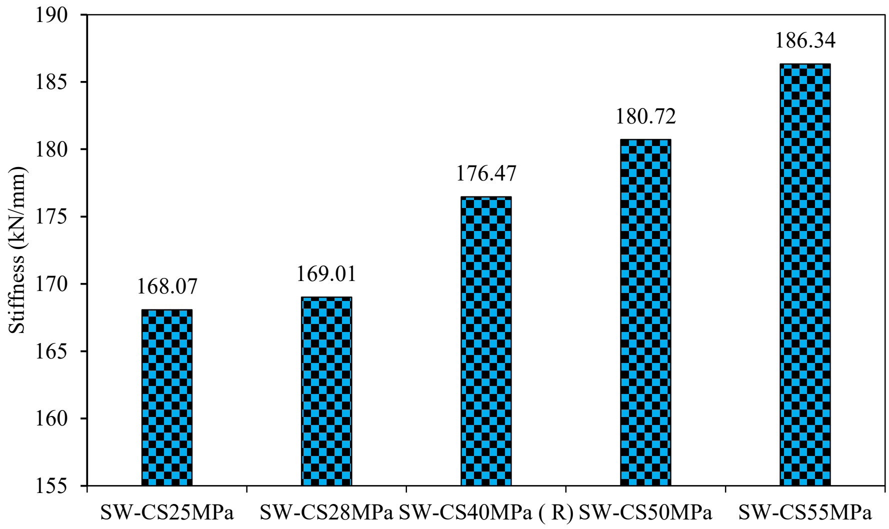

Figure 15. Stiffness of group 2.

3. Ductility

Figure 16 shows that the ductility ratio of the model SW-CS25MPa and SW-CS28MPa was small and reached (1.57, 1.56) because of the small deflection at the ultimate load.

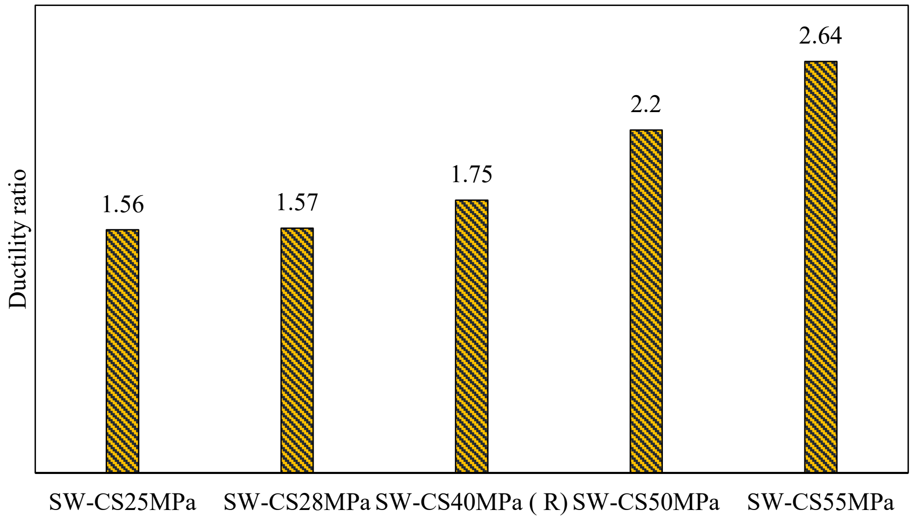

Figure 16. Ductility ratio of group 2.

The models SW-CS50 MPa and SW-CS55 MPa have high deflection values at each of the yield and ultimate load, which made the model ductility ratio reached of moderate value (2.2, 2.64) and caused the gradual drop of the load-deflection curve after the ultimate load.

4. Energy Absorption

The energy absorption of each model through each phase is shown in Figure 17. For SW-CS25MPa and SW-CS28MPa in phase C, when there is a decrease in compressive strength of the concrete wall, the energy absorption decreased by 37 and 3% as compared to the reference model SW-CS45MPa (R). For SW-CS50MPa and SW-CS55MPa in phase C, when there is an increase in compressive strength of the concrete wall, the energy absorption increased by 15 and 25% as compared to the reference model SW-CS45MPa (R).

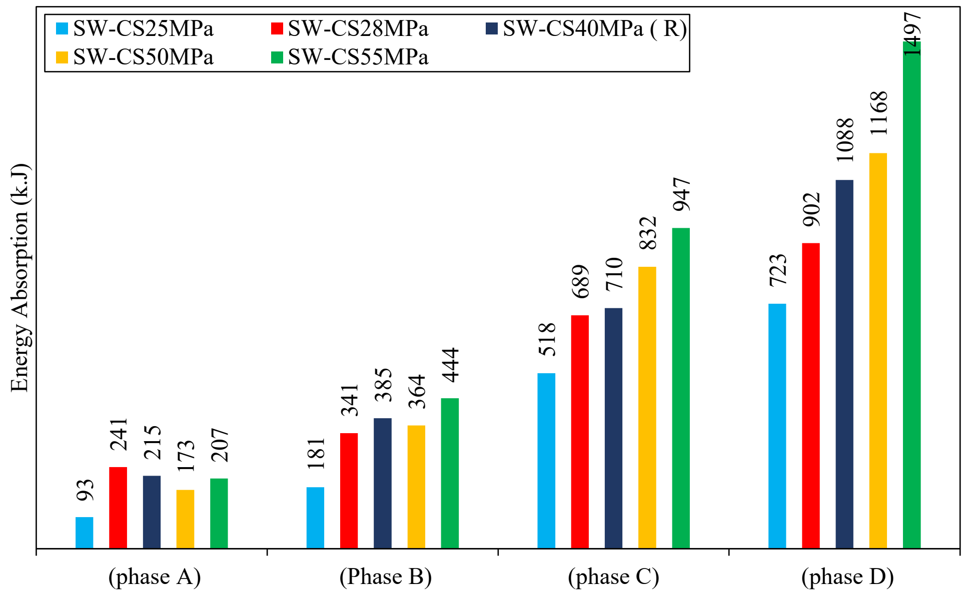

Figure 17. Energy absorption of group 2.

Through phase D, it is noticed that decreased compressive strength of the concrete wall decreased the energy absorption (by 49, 21%) for SW-CS25MPa and SW-CS28MPa as compared with the reference model SW-CS45MPA (R). When increased, the compressive strength of the concrete wall increased the energy absorption (by 8, 28%) for SW-CS50MPa and SW-CS55MPA as compared with reference model SW-CS45MPa (R).

Models with a large value of compressive strength (SW-CS50MPa and SW-CS55MPa) have good energy absorption due to the high area under the curve of load-deflection, and it increases the resistance of the model to the deformation.

From the calculation of stiffness, ductility and energy absorption, it is noticed that the compressive strength of concrete wall has a good effect on the behaviour of smart CSPSW because increasing compressive strength leads to an increase in the contribution of concrete in force transfer; therefore, the influence of lateral load on the infill steel plate becomes low, and also increased compressive strength leads to restricting the model and reducing the lateral offset. From the above results, it is noticed that the compressive strength of a concrete wall should be limited by a specific value (max. 55 MPa) if we want to get more resistance from the concrete wall. Therefore, researchers should change the type of concrete from ordinary to high strength concrete, and this becomes costlier.

4.1.3. The Third Group Models (Influence of Yield Stress of Infill Steel Plate)

1. Lateral displacement

Figure 18 discusses the behaviour of the third group of models (SW-YS150MPa, SW-YS200MPa, SW-YS350MPa and SW-YS380MPa) when gradually experiencing load increases. The out-of-plane displacement of each model generated after the FEM simulation is also demonstrated in Figure 19. The linear and nonlinear behaviour of the models are discussed below:

- Phase A:

For the model SW-YS150MPa and SW-YS200MPa, this phase is characterised by a high increase in the applied loads with a large increase in the model lateral displacement and continual yield displacement (equal to 2.47 and 2.28 mm) for both models. From this, it is noted that the decreasing of the material properties of steel plate represented by yield stress decreased the values of the yield displacement significantly and led to a decrease in the elastic phase.

For the models SW-YS350MPa and SW-YS380MPa, this phase was characterised by a very high increase in the applied loads with a low increase in the model lateral displacement and continual yield displacement (equal to 1.41 and 0.93 mm) for both models. From this, it is noted that the increase in the material properties of steel plate represented by yield stress increased the values of the yield displacement significantly and led to an increase in the elastic phase.

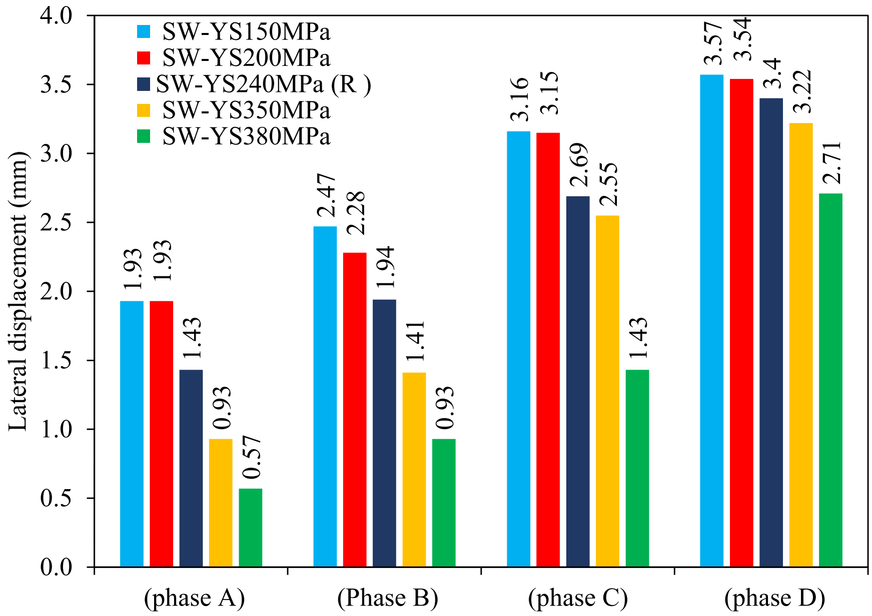

Figure 18. Lateral displacement of group 3.

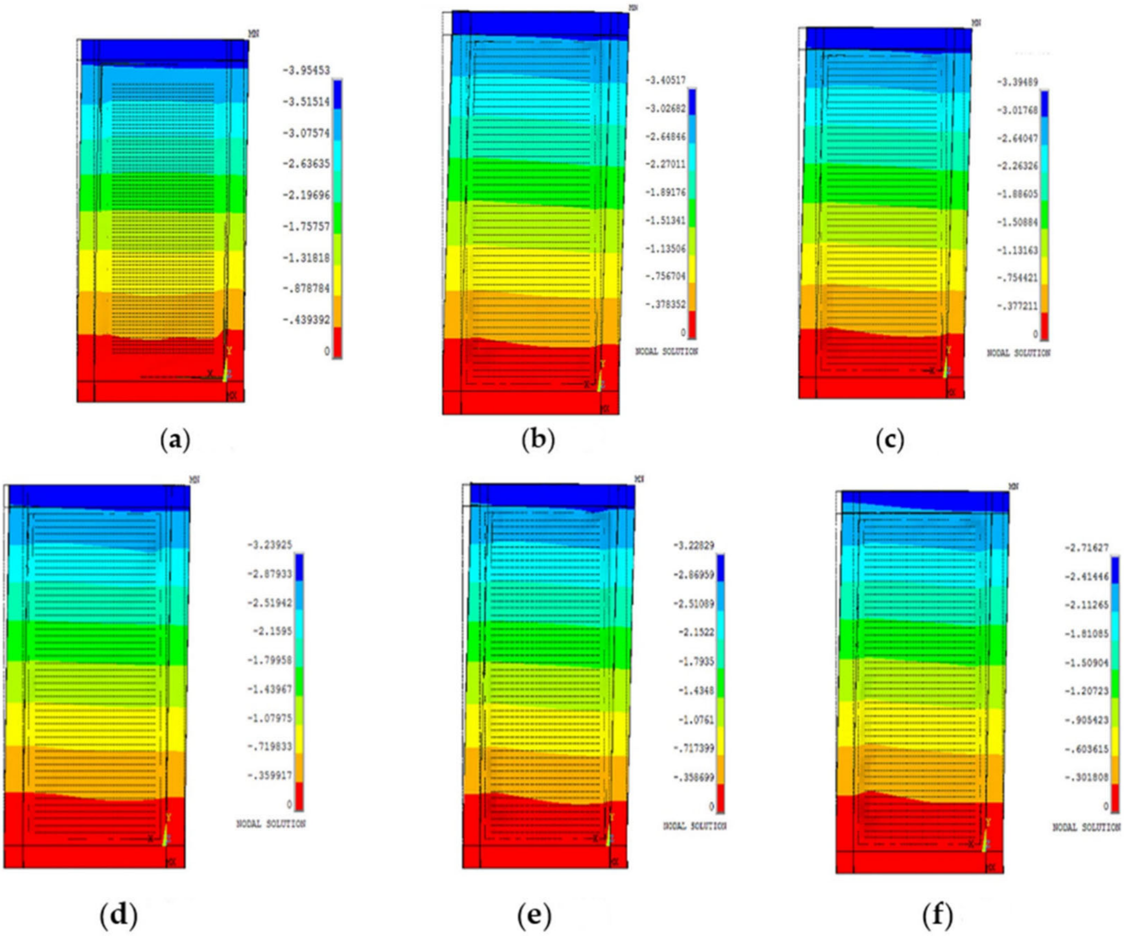

Figure 19. Effect of yield stress (YS) of infill steel plate on the lateral displacement, (**a**) YS = 150 MPa, (**b**) 200 MPa, (**c**) YS = 240 MPa, (**d**) YS = 300 MPa, (**e**) YS = 350 MPa, (**f**) YS = 380 MPa.

- Phase B:

For models SW-YS150MPa and SW-YS200MPa, this phase is characterised by the curve transformation from a straight line with a few inclines to a flat line with a high incline as a result of the high increase in the model displacement as compared with the small increase in the model loads. It has been noted that the decreased material properties of steel plate represented by yield stress are directly proportional to the model's lateral displacement; therefore, the models with low yield stress possessed low resistance compared with the reference model SW-YS240MPa (R).

For models SW-YS350MPa and SW-YS380MPa, it is noted that increased material properties of steel plate represented by yield stress are directly proportional to the model lateral displacement; therefore, the models with high yield stress possessed high resistance compared with the reference model SW-YS240MPa (R).

- Phase C:

In this phase, when decreasing the yield stress (from 240 to 150 MPa) for SW-YS150MPa and SW-YS200MPa, the lateral displacement was larger (by 15, 14.6%) as compared with the reference model SW-YS240MPa (R), where this large displacement led to a sudden drop in the model. When increasing the yield stress (from 240 to 380 MPa) for SW-YS350MPa and SW-YS380MPa, the lateral displacement was lower (by 6 and 88%) as compared with the reference model SW-YS240MPa (R).

- Phase D:

In this phase, for the model SW-YS150MPa, SW-YS200MPa and SW-YS350MPa have very similar behaviour with very close values of the lateral displacement, as shown in Figure 17. From this, it is noted that yield stress value (between 150 and 350 MPa) did not have a large effect on the pre-failure phase for these models. For the model SW-YS380MPa (with yield stress 380), MPa has a good effect on the pre-failure phase.

The collapse of the models SW-YS150MPa and SW-YS200MPa began before reference model SW-YS240MPa (R), while the collapse of SW-YS350MPa and SW-YS380MPa began after reference model SW-YS240MPa (R). Continuing the model loading worked on the development of pure shear yield in the steel plate. From this, it appears that increasing the yield stress of concrete wall delays the failure of smart CSPSW.

2. Stiffness

Figure 20 gives the stiffness values for the seventh group of models, which shows that the stiffness is directly proportional to the increased yield stress of the steel plate. The model SW-YS380MPa, with yield stress equal to 380 MPa, has a high stiffness up to 221.4 kN/mm because of the small lateral displacement at ultimate load, whereas the model SW-YS150MPa, with yield stress equal to 150 MPa, has a low stiffness equal to 168.07 kN/mm because of its high lateral displacement at the ultimate load.

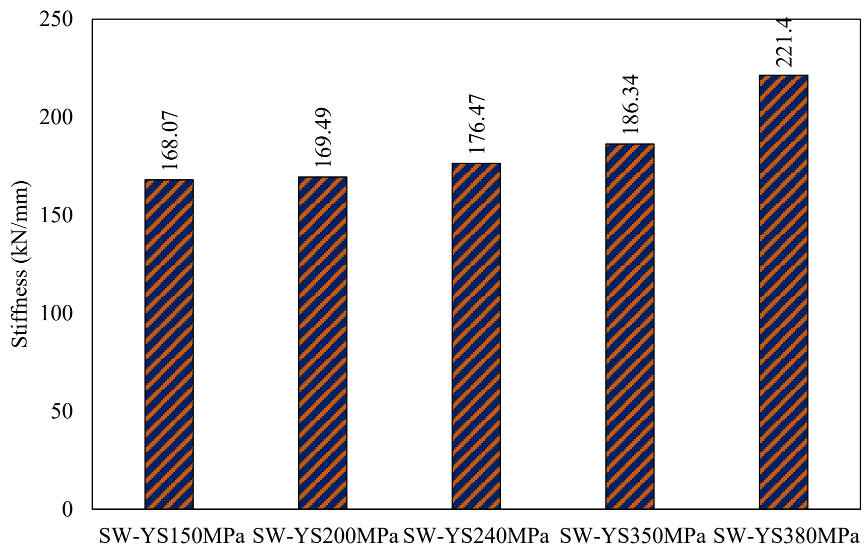

Figure 20. Stiffness of group 3.

3. Ductility

Figure 21 demonstrates that the ductility of the model SW-YS150MPa and SW-YS200MPa was very low (and reached 1.45, 1.56) because of the small deflection at the ultimate load. These few data caused the rapid and sudden drop in the load-carrying capacity when this model arrived at the ultimate load compared with the gradual drop of the reference model SW-YS240MPa (R). While the models SW-YS350MPa and SW-YS380MPa had high deflection values at each of the yield and ultimate load (which made the model ductility of moderate value reach 2.28, 2.91), this caused the gradual drop of the load-deflection curve after the ultimate load.

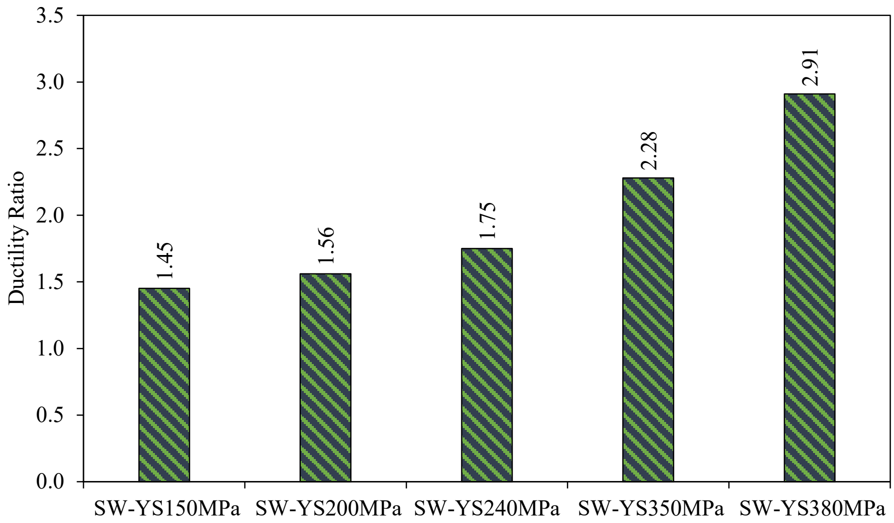

Figure 21. Ductility ratio of group 3.

4. Energy Absorption

The energy absorption of each model through each phase is shown in Figure 22 for SW-YS150MPA, SW-YS200MPA and SW-YS350MPA in phase C. When the yield stress of the steel plate is equal to 150,200 and 380 MPa, the energy absorption decreases (by 27, 9 and 41%) as compared to the reference model SW-YS240MPa (R). For SW-YS380MPa in phase C, when the yield stress of steel plate is equal to 350 MPa, the energy absorption increased (by 0.21%) as compared to reference model SW-YS240MPa (R).

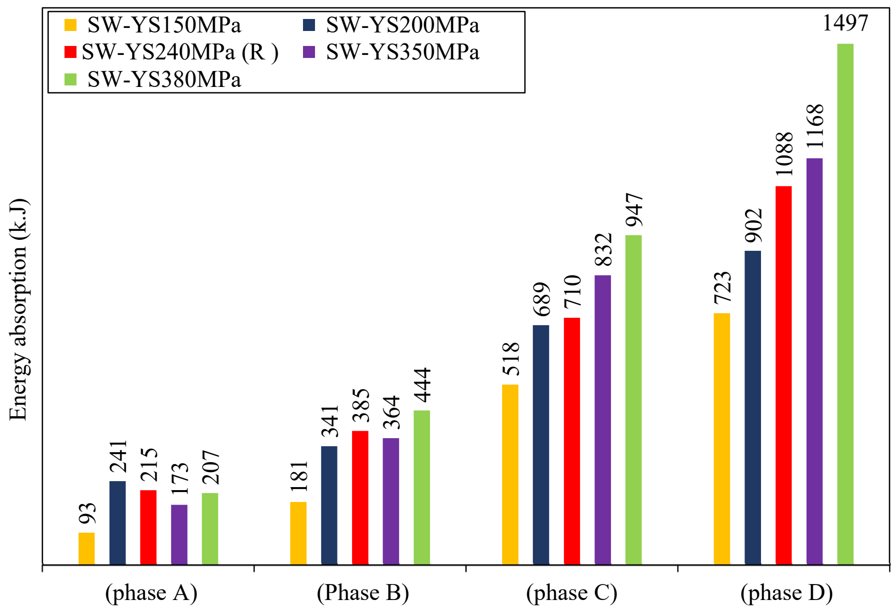

Figure 22. Energy absorption of group 3.

Through phase D, it is noticed that the decreased yield stress of steel plate decreases the energy absorption (by 42 and 29%) for SW-YS150MPa and SW-YS200MPa as compared with the reference model SW-YS240MPa®. When the yield stress of steel plates is increased, the energy absorption increases (by 15, 12%) for SW-YS350MPa and SW-YS380MPa as compared with the reference model SW-YS240MPa (R). The models with a large value of yield stress (SW-YS350MPa) have a small effect on energy absorption.

From the calculation of stiffness, ductility and energy absorption, it is observed that the yield stress of the steel plate has a good effect on the behaviour of smart CSPSW because increasing yield stress leads to an increase in the contribution of steel plate in resistance to lateral displacement. Therefore, the influence of lateral load on the concrete wall becomes low; besides this, increasing the yield stress leads to a decrease the critical force and average buckling stresses.

From the results of the phases above, it is noticed that the yield stress of steel plate should be limited by a specific value (max. 350 MPa); this is because to get greater resistance of steel plate, there should be a change in the type of steel plate, and this becomes costlier. Furthermore, the behaviour of smart CSPSW remains the same beyond that value of the yield stress.

4.1.4. The Fourth Group Models (Influence of Shear Stud Layout)

1. Lateral displacement

From Figure 23, it is observed that the models SW-L8*3, SW-L6*4, SW-L4*6, SW-L2*12 and SW-L12*2 went through the same phase of the reference model SW-L3*8 (R) when unloaded gradually and this has been discussed in detail below. Additionally, the out-of-plane displacement of each model from group 4 is shown in Figure 24.

- Phase A:

For the models SW-L8*3, SW-L6*4, SW-L4*6, SW-L2*12 and SW-L12*2, the elastic phase started from the beginning of loading to yield displacement (equal to 1.42, 1.52, 1.43, 1.43, 1.41 mm, respectively) and is characterised by a linear relationship between the applied load and the model displacement.

In this phase, the lateral displacement values of the models SW-L8*3, SW-L6*4, SW-L4*6, SW-L2*12 and SW-L12*2 were lower (by 47, 42, 49, 51, 52%) as compared with the reference model SW-L3*8 (R), as shown in Figure 21, as a result of a change in the layout of the shear stud of smart CSPSW which causes the decrease in the yield displacement and increase in the yield load values that lead to increase the elastic stage for all the models as compared to reference model SW-L3*8 (R). From this, it is noted that the layout of the shear stud has no large effect on the elastic phase for these models.

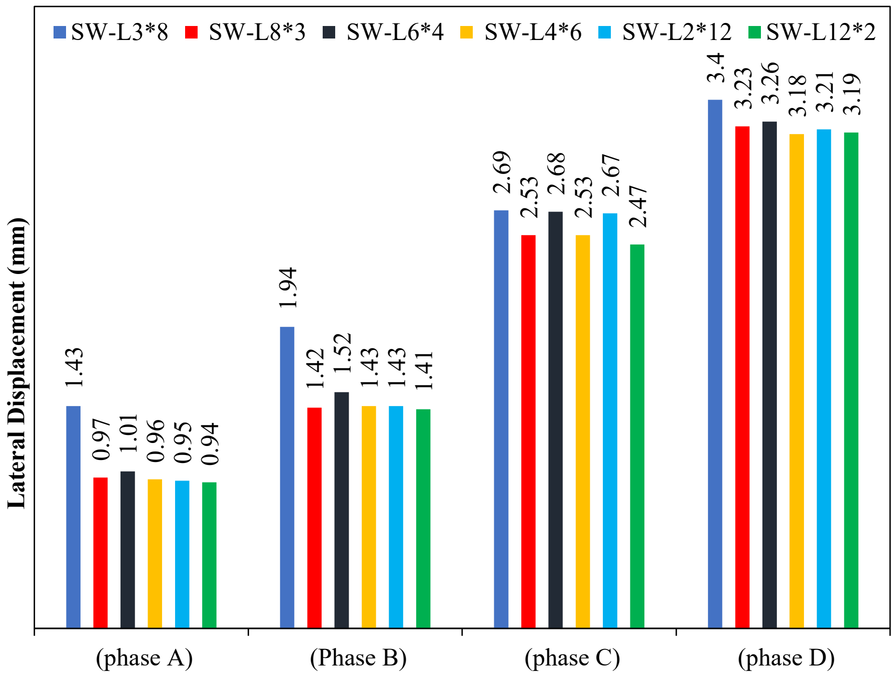

Figure 23. Lateral displacement of group 4.

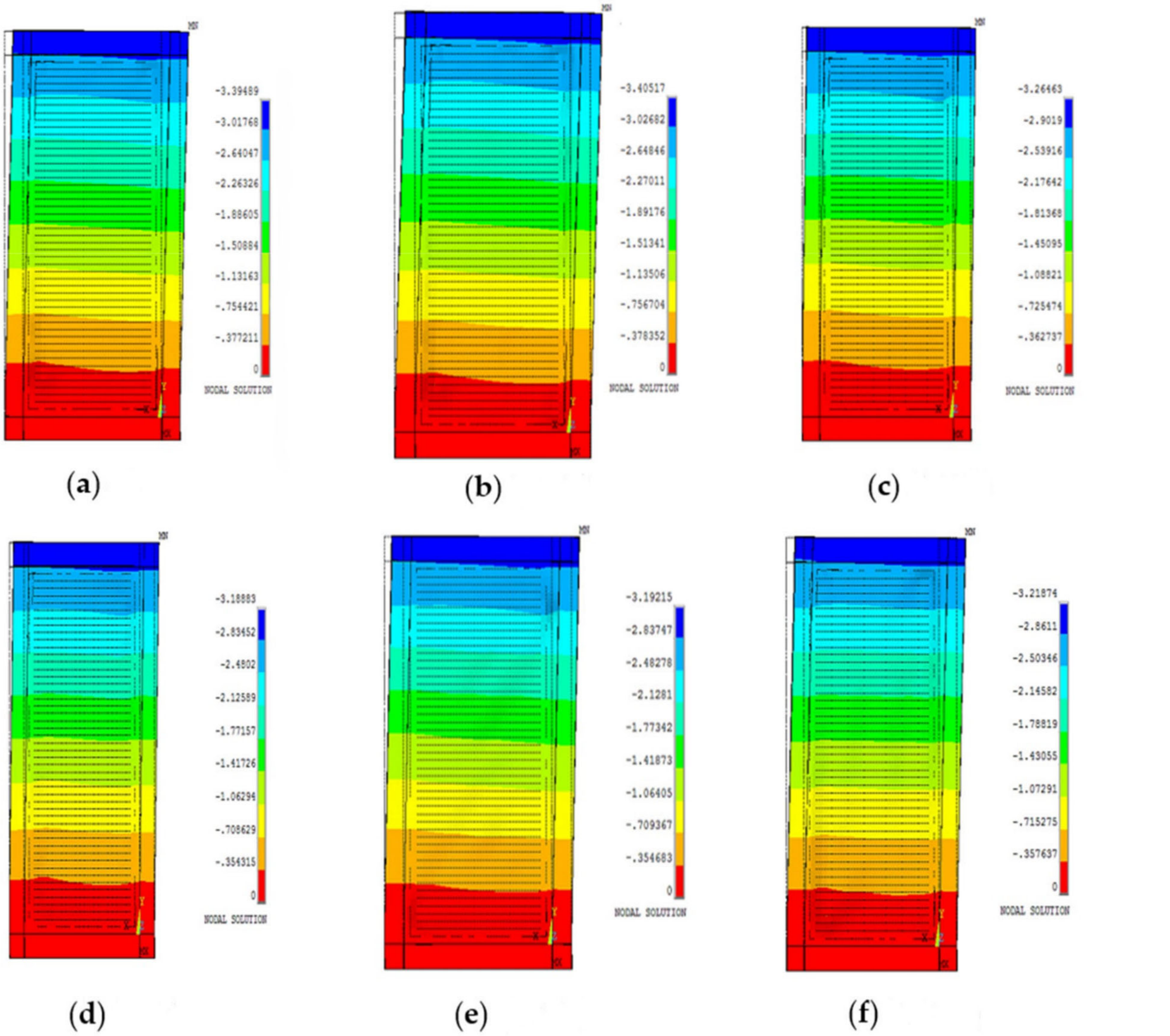

Figure 24. Effect of shear stud layout on the lateral displacement. (**a**) (3 × 8), (**b**) (8 × 3), (**c**) (4 × 6), (**d**) (6 × 4), (**e**) (2 × 12), (**f**) (12 × 2).

- Phase B:

This stage involves the start of the plastic model behaviour. Here, a small increment occurs in the applied loads contrasted and a high increment in lateral displacement, and this proceeded until it reached to the ultimate load. The shear yield zone of the model SW-L8*3, SW-L6*4, SW-L4*6, SW-L2*12 and SW-L12*2 was larger than (by 37, 28, 36, 36, 38) % as compared to the reference model SW-L3*8 (R).

From this, it is noted that the change in the layout of shear stud becomes more effective when it is concentrated horizontally more than vertically and this enhances the behaviour of smart CSPSW. Thus, it significantly affected the shear yield phase through the escalation of the strain hardening capacity which leads to a significant escalation of the models' stress redistribution compared to the reference model SW-L3*8 (R).

- Phase C:

In this phase, all models of the eighth group had very similar behaviour with very close values of the lateral displacement. It is noted that the change in the layout of the shear stud in the CSPSW models did not have a substantial effect on the post shear yielding phase for these models. In this phase, when there was variation in the layout of shear stud for SW-L8*3, SW-L6*4, SW-L4*6, SW-L2*12 and SW-L12*2, the lateral displacement was lower (by 7, 0.37, 6.32, 0.75, 9%) as compared to the reference model SW-L3*8 (R).

- Phase D:

This phase began with the arrival of the model at the ultimate load by exposure of all model elements situated above and below the shear stud to high stresses. The collapse of the reference model SW-L3*8 (R) began with the occurrence of buckling in the infill steel plate because of the use of the maximum layout of shear studs in the vertical direction, in other words, a low number of shear studs in the horizontal direction led to reducing the restricted model. After comparison of the result in this phase at the same cycle loading, it is noticed that the lateral displacement of SW-L8*3, SW-L6*4, SW-L4*6, SW-L2*12 and SW-L12*2 was lower (by 5, 4.29, 6.92, 5.92, 6.58%) as compared with the reference model SW-L3*8 (R).

2. Stiffness

Figure 25 shows the values of the stiffness for the eight group models. Figure 25 displays that change in the layout of shear stud in the models SW-L8*3, SW-L6*4, SW-L4*6, SW-L2*12 and SW-L12*2 enhances their stiffness (by 5, 4.12, 6.47, 5.59, 6.18%, respectively) compared with the reference model SW-L3*8 (R) because of the small lateral displacement of these models. From these stiffness values, it is noted that the change in the layout of the shear stud has the smallest effect on the model stiffness.

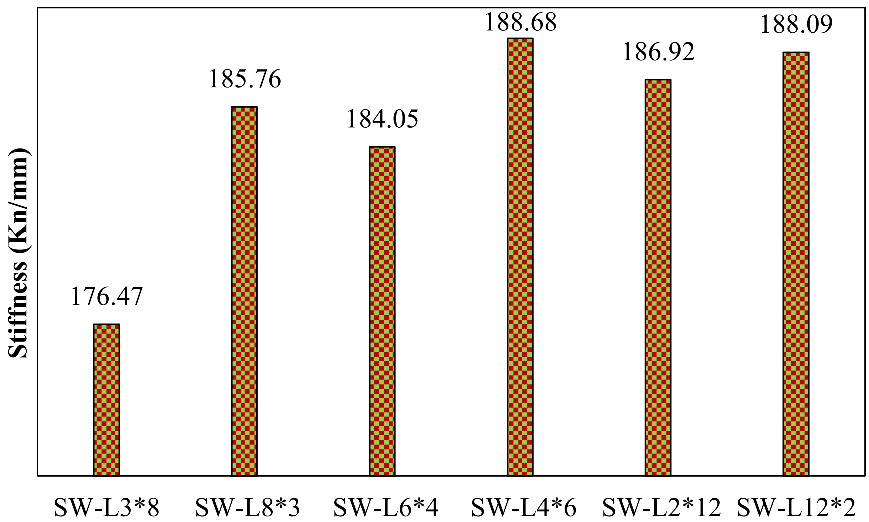

Figure 25. Stiffness of group 4.

3. Ductility

Figure 26 shows the ductility values of the eight group models. From this figure, it is noted that the increased distance between shear studs in the models SW-L8*3, SW-L6*4, SW-L4*6, SW-L2*12 and SW-L12*2 enhances their ductility significantly (by 22.91, 18.22, 21.17, 21.88 and 22.57%, respectively) as compared with the reference model SW-L3*8 (R).

This is because of the high upgrade in the values of lateral load for these models. Consequently, it was seen that there is a continuous drop in the load-carrying capacity of these models and a sudden and fast drop in the reference model SW-L3*8 (R).

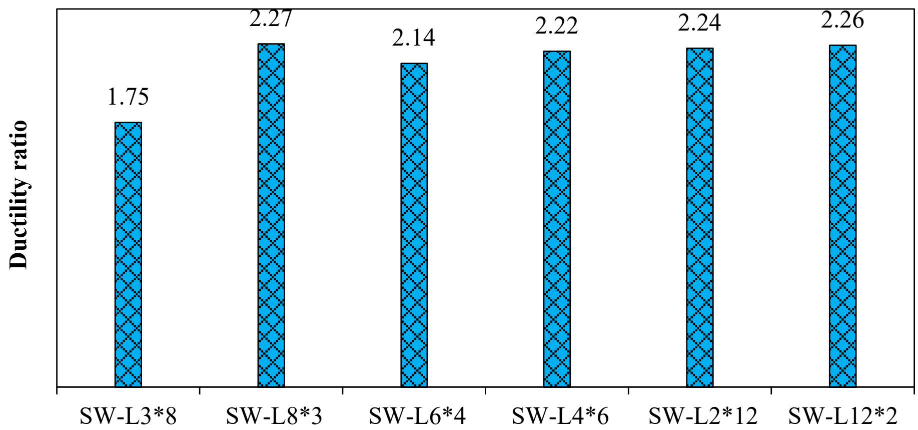

Figure 26. Ductility ratio of group 4.

4. Energy Absorption

Figure 27 show the results of energy absorption of each model through each phase. For SW-L8*3, SW-L6*4, SW-L4*6, SW-L2*12 and SW-L12*2 in phase C, when changing the layout of the shear stud, the energy absorption increased (by 11.03, 16.17, 22.83, 25.18 and 20.94%) as compared with reference model SW-L3*8 (R). Through the phase D, it is noticed that change in the layout of the shear stud increased the energy absorption (by 5.23, 4.31, 15.59, 13.38 and 16.56%) for SW-L8*3, SW-L6*4, SW-L4*6, SW-L2*12 and SW-L12*2 as compared with reference model SW-L3*8 (R).

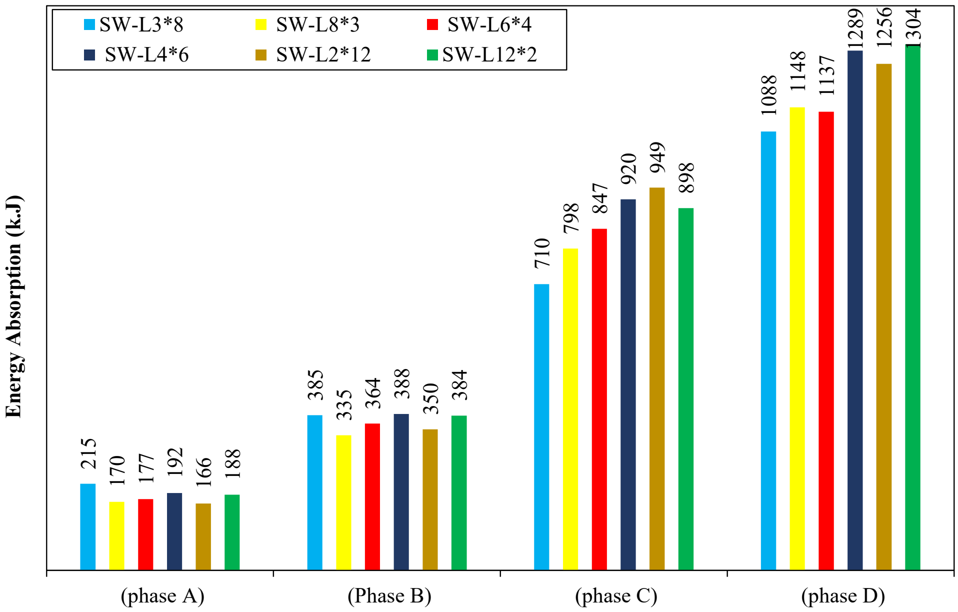

Figure 27. Energy absorption of group 4.

Models with layout (12 × 2) (horizontal × vertical) (SW-L12*2) have excellent energy absorption, due to the high area under the curve of load-deflection, and this refers to an increase in the resistance of the model to the deformation. From the results of stiffness, ductility and energy absorption, it is noticed that the layout of the shear stud should be a concentrated distribution of the vertical to the horizontal direction, because large distances will cause widespread buckling of the steel plate in free subpanels between shear studs and would result in no improvement. Therefore, the layout of the shear stud was (12 × 2, 6 × 4) (horizontal × vertical).

5. Conclusions

The present approach provides a practical way to model the complex geometry of steel-concrete composite shear walls by using ANSYS. This study has discussed the numerical attributes of shear walls and presented parametric effects of different reinforcement ratios, the compressive strength of the concrete wall, the layout of shear stud and the yield stress of infill steel plate on the lateral resisting capacities.

The nonlinear cyclic behaviour of the shear walls with steel and concrete acting together is investigated with reference to earlier test data. The predicted deformation-load values are compared with the experimental results using hysteric curves to check the compatibility of the technique.

A good agreement is shown between the numerical and experimental hysteric curve as a response of reversed loading. Furthermore, based on the numerical result conducted in this study, the researchers concluded the following:

1. The ratio of reinforcement has a good effect on the behaviour of smart CSPSW because the increasing ratio of reinforcement leads to a gradual drop in the load-carrying capacity until it reaches the fracture load. The ratio of reinforcement walls should be limited by a specific value, max. 3.5%, because the behaviour of smart CSPSW remains the same beyond that ratio (so the best range for using the thickness of the concrete wall was 1–3.5%).
2. The compressive strength of the concrete walls has a vital impact on the behaviour of smart CSPSW. Increasing compressive strength leads to an increase in the contribution of concrete in force transfer. Therefore, the influence of lateral load on the infill steel plate becomes low. Additionally, increasing compressive strength led to restricting the model and reducing the lateral offset. The compressive strength of concrete walls should be limited by a specific value (max. 55 MPa). This is because to obtain more resistance from the concrete walls, there should be a change in the grade of concrete from ordinary to high strength, and this becomes costlier.
3. The yield stress of steel plate should be limited by a specific value (max. 350 MPa); this is because to obtain more resistance from steel plate, we should change the type of steel plate, and this becomes costlier. Additionally, the behaviour of smart CSPSW remains the same beyond that value of yield stress. The change in the layout of the shear stud affected the type of failure in the model. The layout of the shear stud should be a concentrated distribution of the vertical to the horizontal direction. Since large distances will cause widespread buckling of the steel plate in free subpanels between shear studs and would result in no improvement, a layout of the shear studs was selected of (12×2, 6×4) (horizontal $\times$ vertical).

Author Contributions: Conceptualisation, H.M.N., A.M.I., M.M.S., A.H., S.M., N.S.M., M.M.A.E. and K.M.K.; methodology, H.M.N., A.M.I., M.M.S., A.H., S.M., N.S.M., M.M.A.E. and K.M.K.; software, H.M.N., A.M.I., M.M.S., A.H., S.M., N.S.M., M.M.A.E. and K.M.K.; validation, H.M.N., A.M.I., M.M.S., A.H., S.M., N.S.M., M.M.A.E. and K.M.K.; formal analysis, H.M.N., A.M.I., M.M.S., A.H., S.M., N.S.M., M.M.A.E. and K.M.K.; investigation, H.M.N.; resources, M.M.S.; data curation, H.M.N., A.M.I., M.M.S., A.H., S.M., N.S.M., M.M.A.E. and K.M.K.; writing—original draft preparation, H.M.N. and A.M.I.; writing—review and editing, H.M.N., A.M.I., M.M.S., A.H., S.M., N.S.M., M.M.A.E. and K.M.K.; visualisation, H.M.N., A.M.I., M.M.S., A.H., S.M., N.S.M., M.M.A.E. and K.M.K.; supervision, H.M.N. and A.M.I.; project administration, M.M.S.; funding acquisition, M.M.S. All authors have read and agreed to the published version of the manuscript.

Funding: The research is partially funded by the Ministry of Science and Higher Education of the Russian Federation as part of the World-class Research Center program: Advanced Digital Technologies (contract No. 075-15-2022-311 dated 20 April 2022). This research work was supported by the Deanship of Scientific Research at King Khalid University/Abha/Saudi Arabia under Grant number RGP. 2/246/43.

Institutional Review Board Statement: Not applicable.

Informed Consent Statement: Not applicable.

Data Availability Statement: Not applicable.

Acknowledgments: The authors extend their thanks to the Deanship of Scientific Research at King Khalid University/Abha/Saudi Arabia for supporting this work. Additionally, the authors extend their thanks to the Ministry of Science and Higher Education of the Russian Federation for funding this work.

Conflicts of Interest: The authors declare no conflict of interest.

References

1. Ji, X.; Cheng, Y.; Leong, T.; Cui, Y. Seismic Behavior and Strength Capacity of Steel Coupling Beam-to-SRC Wall Joints. *Eng. Struct.* **2019**, *201*, 109820. [CrossRef]
2. González, J.G.; Hernández-Ortega, J.J.; Jiménez-Ballesta, A.E.; Pedreño, R.Z. Analysis of Tube-to-Tubesheet Welding in Carbon Steel Heat Exchangers of a Double Plate Header Box. *Materials* **2022**, *15*, 261. [CrossRef] [PubMed]
3. Zhao, J.; Cai, G.; Si Larbi, A.; Zhang, Y.; Dun, H.; Degée, H.; Vandoren, B. Hysteretic Behaviour of Steel Fibre RC Coupled Shear Walls under Cyclic Loads: Experimental Study and Modelling. *Eng. Struct.* **2018**, *156*, 92–104. [CrossRef]
4. Wang, B.; Jiang, H.; Lu, X. Experimental and Numerical Investigations on Seismic Behavior of Steel Truss Reinforced Concrete Core Walls. *Eng. Struct.* **2017**, *140*, 164–176. [CrossRef]
5. Jiang, D.; Xiao, C.; Chen, T.; Zhang, Y. Experimental Study of High-Strength Concrete-Steel Plate Composite Shear Walls. *Appl. Sci.* **2019**, *9*, 2820. [CrossRef]
6. Hassan, A.; Arif, M.; Shariq, M.; Alomayri, T. Experimental Test and Finite Element Modelling Prediction on Geopolymer Concrete Beams Subject to Flexural Loading. *Innov. Infrastruct. Solut.* **2022**, *7*, 13. [CrossRef]
7. Wang, K.; Zhang, W.; Chen, Y.; Ding, Y. Seismic Analysis and Design of Composite Shear Wall with Stiffened Steel Plate and Infilled Concrete. *Materials* **2022**, *15*, 182. [CrossRef]
8. Dan, D.; Fabian, A.; Stoian, V. Theoretical and Experimental Study on Composite Steelconcrete Shear Walls with Vertical Steel Encased Profiles. *J. Constr. Steel Res.* **2011**, *67*, 800–813. [CrossRef]
9. Lu, X.; Zhang, Y.; Zhang, H.; Zhang, H.; Xiao, R. Experimental Study on Seismic Performance of Steel Fiber Reinforced High Strength Concrete Composite Shear Walls with Different Steel Fiber Volume Fractions. *Eng. Struct.* **2018**, *171*, 247–259. [CrossRef]
10. Ramesh, S. *Behavior and Design of Earthquake-Resistant Dual-Plate Composite Shear Wall Systems*; Purdue University: West Lafayette, IN, USA, 2013.
11. Bruneau, M.; Alzeni, Y.; Fouché, P. Seismic Behavior of Concrete-Filled Steel Sandwich Walls and Concrete-Filled Steel Tube Columns. In Proceedings of the Steel Innovations Conference 2013, Christchurch, New Zealand, 21–22 February 2013.
12. Yan, J.B.; Yan, Y.Y.; Wang, T. Cyclic Tests on Novel Steel-Concrete-Steel Sandwich Shear Walls with Boundary CFST Columns. *J. Constr. Steel Res.* **2020**, *164*, 105760. [CrossRef]
13. Liu, Y.; Zhou, Z.; Cao, W.; Wei, L. Study on Seismic Performance of the Masonry Wall with Lightweight Concrete Filled Steel Tube Core Column and Thermal-Insulation Sandwich. *J. Earthq. Eng. Eng. Vib.* **2016**, *15*, 223–230. [CrossRef]
14. *ASCE/SEI 7-2022*; Minimum Design Loads for Buildings and Other Structures. American National Standards Institute: New York, NY, USA, 2022.
15. AISC American Institute of Steel Construction. *Seismic Provisions for Structural Steel Buildings*; American Institute of Steel Construction: Chicago, IL, USA, 2010.
16. Nie, X.; Wang, J.J.; Tao, M.X.; Fan, J.S.; Bu, F.M. Experimental Study of Flexural Critical Reinforced Concrete Filled Composite Plate Shear Walls. *Eng. Struct.* **2019**, *197*, 109439. [CrossRef]
17. Othuman Mydin, M.A.; Wang, Y.C. Structural Performance of Lightweight Steel-Foamed Concretesteel Composite Walling System under Compression. *Thin-Walled Struct.* **2011**, *49*, 66–76. [CrossRef]
18. Wright, H. Axial and Bending Behavior of Composite Walls. *J. Struct. Eng.* **1998**, *124*, 758–764. [CrossRef]
19. Wang, M.Z.; Guo, Y.L.; Zhu, J.S.; Yang, X. Flexural-Torsional Buckling and Design Recommendations of Axially Loaded Concrete-Infilled Double Steel Corrugated-Plate Walls with T-Section. *Eng. Struct.* **2020**, *208*, 110345. [CrossRef]
20. Zhang, X.; Qin, Y.; Chen, Z. Experimental Seismic Behavior of Innovative Composite Shear Walls. *J. Constr. Steel Res.* **2016**, *116*, 218–232. [CrossRef]
21. Zhang, W.; Wang, K.; Chen, Y.; Ding, Y. Experimental Study on the Seismic Behaviour of Composite Shear Walls with Stiffened Steel Plates and Infilled Concrete. *Thin-Walled Struct.* **2019**, *144*, 106279. [CrossRef]
22. Najem, H.M. Influence of Concrete Strength on the Cycle Performance of Composite Steel Plate Shear Walls. *Diyala J. Eng. Sci.* **2018**, *11*, 1–7. [CrossRef]
23. Najem, H.M. The Effect of Infill Steel Plate Thickness on the Cycle Behavior of Steel Plate Shear Walls. *Diyala J. Eng. Sci* **2018**, *11*, 1–6. [CrossRef]
24. Nguyen, N.H.; Whittaker, A.S. Numerical Modelling of Steel-Plate Concrete Composite Shear Walls. *Eng. Struct.* **2017**, *150*, 1–11. [CrossRef]

25. Epackachi, S.; Whittaker, A.S.; Varma, A.H.; Kurt, E.G. Finite Element Modeling of Steel-Plate Concrete Composite Wall Piers. *Eng. Struct.* **2015**, *100*, 369–384. [CrossRef]
26. Rafiei, S.; Hossain, K.M.A.; Lachemi, M.; Behdinan, K.; Anwar, M.S. Finite Element Modeling of Double Skin Profiled Composite Shear Wall System under In-Plane Loadings. *Eng. Struct.* **2013**, *56*, 46–57. [CrossRef]
27. Wei, F.F.; Zheng, Z.J.; Yu, J.; Wang, Y.Q. Computational Method for Axial Compression Capacity of Double Steel-Concrete Composite Shear Walls with Consideration of Buckling. *Gongcheng Lixue Eng. Mech.* **2019**, *36*, 154–164. [CrossRef]
28. Guo, L.; Wang, Y.; Zhang, S. Experimental Study of Rectangular Multi-Partition Steel-Concrete Composite Shear Walls. *Thin-Walled Struct.* **2018**, *130*, 577–592. [CrossRef]
29. Wang, M.Z.; Guo, Y.L.; Zhu, J.S.; Yang, X. Flexural Buckling of Axially Loaded Concrete-Infilled Double Steel Corrugated-Plate Walls with T-Section. *J. Constr. Steel Res.* **2020**, *166*, 105940. [CrossRef]
30. Shafaei, S.; Ayazi, A.; Farahbod, F. The Effect of Concrete Panel Thickness upon Composite Steel Plate Shear Walls. *J. Constr. Steel Res.* **2016**, *117*, 81–90. [CrossRef]
31. Qin, Y.; Shu, G.P.; Zhou, G.G.; Han, J.H. Compressive Behavior of Double Skin Composite Wall with Different Plate Thicknesses. *J. Constr. Steel Res.* **2019**, *157*, 297–313. [CrossRef]
32. Huang, Z.; Liew, J.Y.R. Structural Behaviour of Steel-Concrete-Steel Sandwich Composite Wall Subjected to Compression and End Moment. *Thin-Walled Struct.* **2016**, *98*, 592–606. [CrossRef]
33. Li, X.; Li, X. Steel Plates and Concrete Filled Composite Shear Walls Related Nuclear Structural Engineering: Experimental Study for out-of-Plane Cyclic Loading. *Nucl. Eng. Des.* **2017**, *315*, 144–154. [CrossRef]
34. Epackachi, S.; Nguyen, N.H.; Kurt, E.G.; Whittaker, A.S.; Varma, A.H. In-Plane Seismic Behavior of Rectangular Steel-Plate Composite Wall Piers. *J. Struct. Eng.* **2015**, *141*, 04014176. [CrossRef]
35. *JGJ/T 380*; Technical Specification for Steel Plate Shear Walls. Ministry of Housing and Urban-Rural Development: Beijing, China, 2015.
36. *ACI 318M-11*; Building Code Requirements for Structural Concrete and Commentary. ACI Committee 318: Farmington Hills, MI, USA, 2011.
37. *ANSI/AISC N690-18*; Specification for Safety-Related Steel Structures for Nuclear Facilities. American Institute of Steel Construction: Chicago, IL, USA, 2018.
38. Epackachi, S.; Nguyen, N.H.; Kurt, E.G.; Whittaker, A.S.; Varma, A.H. An Experimental Study of the In-Plane Response of Steel-Concrete Composite Walls. In Proceedings of the 22nd International Conference on Structural Mechanics in Reactor Technology (SMiRT-22), San Francisco, CA, USA, 18 August 2013.
39. Khatir, S.; Tiachacht, S.; le Thanh, C.; Ghandourah, E.; Mirjalili, S.; Abdel Wahab, M. An Improved Artificial Neural Network Using Arithmetic Optimization Algorithm for Damage Assessment in FGM Composite Plates. *Compos. Struct.* **2021**, *273*, 114287. [CrossRef]
40. Saadatmorad, M.; Jafari-Talookolaei, R.A.; Pashaei, M.H.; Khatir, S. Damage Detection on Rectangular Laminated Composite Plates Using Wavelet Based Convolutional Neural Network Technique. *Compos. Struct.* **2021**, *278*, 114656. [CrossRef]
41. Khatir, S.; Tiachacht, S.; Thanh, C.-L.; Tran-Ngoc, H.; Mirjalili, S.; Abdel Wahab, M. A Robust FRF Damage Indicator Combined with Optimization Techniques for Damage Assessment in Complex Truss Structures. *Case Stud. Constr. Mater.* **2022**, *17*, e01197. [CrossRef]
42. Rahai, A.; Hatami, F. Evaluation of Composite Shear Wall Behavior under Cyclic Loadings. *J. Constr. Steel Res.* **2009**, *65*, 1528–1537. [CrossRef]
43. Zhao, Q.; Astaneh-Asl, A. Cyclic Behavior of Traditional and Innovative Composite Shear Walls. *J. Struct. Eng.* **2004**, *130*, 271–284. [CrossRef]